A unified model of CA1/3 pyramidal cells: An investigation into excitability

Jakub Nowacki[*], Hinke M. Osinga[*], Jon T. Brown[†], Andrew D. Randall[†], Krasimira Tsaneva-Atanasova[*]

May 28, 2010

Abstract

After-depolarisation is a hallmark of excitability in hippocampal pyramidal cells of CA1 and CA3 regions, because it constitutes the subthreshold relation between inward and outward ionic currents. This relationship determines the nominal response to stimuli and provides the necessary conditions for firing a spike or a burst of action potentials. Nervertheless, after-depolarisation is an inherently transient phenomenon that is not very well understood. We study after-depolarisation using a single-compartment pyramidal-cell model based on recent voltage-clamp and current-clamp experimental data. We systematically investigate CA1 and CA3 behaviour and show that changes to maximal conductance of T-type Ca^{2+}-current, muscarinic-sensitive and delayed rectifier K^{+}-currents are sufficient to switch the behaviour of the model from a CA3 to a CA1 neuron. We use model analysis to define after-depolarisation and bursting threshold. We also explain the influence of particular ionic currents on this phenomenon. This study ends with a sensitivity analysis that demonstrates the influence of specific currents on excitability. Counter-intuitively, we find that a decrease of Na^{+}-current could cause an increase in excitability. Our analysis predicts that a change of high-voltage activated Ca^{2+}-current can have a similar effect.

Keywords: Excitability; Mathematical Model; Transient Dynamics; After-depolarisation (ADP); Nullcline; Sensitivity Analysis

1 Introduction

In this paper we study the mechanisms underlying the excitability of the hippocampal pyramidal neurons that are the principal excitatory neurons of the hippocampus. Excitability in neurons is known as the ability to integrate and amplify perturbations received in the form of stimuli, and to produce a spike response (Hodgkin and Huxley, 1952; Izhikevich, 2006). The hippocampus is critical for the formation of new memories and is one of the first brain areas to show damage in Alzheimer's disease. It is also a common focus site in epilepsy that can be damaged through chronic seizures (Andersen et al., 2007). Hence, changes in excitability of neurons in this brain region may have a profound impact on the overall performance of the brain (Brown and Randall, 2009; Harvey et al., 2009; Kile et al., 2008; Misra et al., 2008).

[*]Bristol Centre for Applied Nonlinear Mathematics, Department of Engineering Mathematics, University of Bristol, Queen's Building, University Walk, BS8 1TR

[†]School of Medical Sciences, University of Bristol, University Walk, BS8 1TD

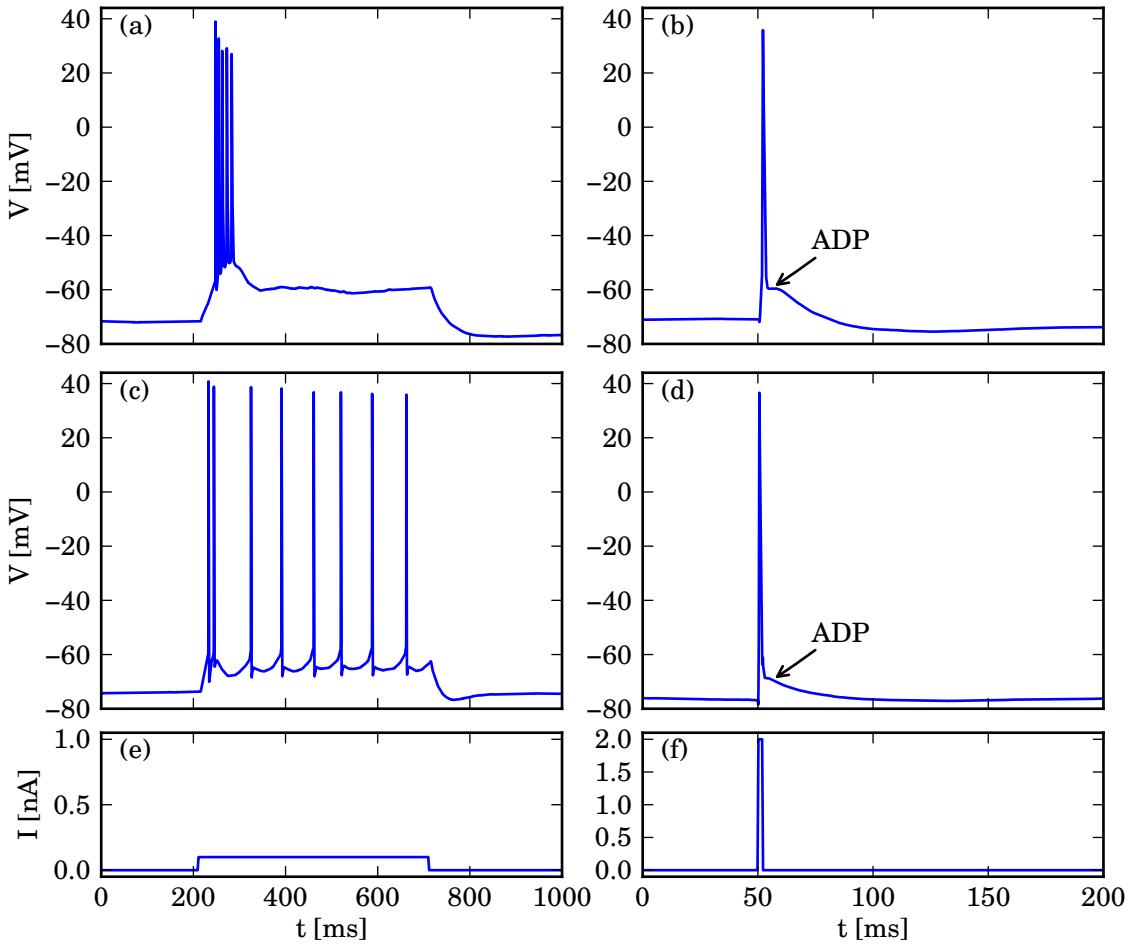

Figure 1: Electrophysiological differences between CA1- and CA3-area neurons; in a long-stimulus experiment 100 pA current is injected into a cell for 500 ms; in a short-stimulus experiment 2 nA current is injected into a cell for 2 ms; panels (a) and (b) show the typical responses of a CA3-area neuron to long and short stimuli, respectively; similarly, panels (c) and (d) show the typical responses of a CA1-area neuron to these two stimuli, respectively; panels (e) and (f) show the time traces of the injected current for the long- and a short-stimulus experiments, respectively.

From an electrophysiological point of view, pyramidal neurons in CA1 and CA3 exhibit noticeably different behaviours; Fig. 1 illustrates examples of the responses for two in-vitro current-clamp experiments. The left column of Fig. 1 presents a long-current injection experiment, where current of magnitude 100 pA (e) is injected into a CA3 (a) and CA1 (c) neuron for the duration of 500 ms. The right column of Fig. 1 presents a short-current injection experiment, where 2 nA current (f) is injected into a CA3 (b) and CA1 (d) neuron for the duration of 2 ms. Pyramidal neurons from the CA3 region are characterised by more versatile behaviour during the long positive-current injection compared with pyramidal neurons from the CA1 region (Andersen et al., 2007; Wong and Prince, 1981; Traub et al., 1991; Scharfman, 1993; Migliore et al.,

1995; Safiulina et al., 2008; Brown and Randall, 2009). Figure 1(a) depicts a common feature of neurons from the CA3 area, that is, a high-frequency burst followed by a depolarised plateau with or without several low-frequency spikes (Andersen et al., 2007; Wong and Prince, 1981; Traub et al., 1991; Scharfman, 1993; Migliore et al., 1995; Safiulina et al., 2008; Brown and Randall, 2009). The frequency of the spikes increases with the amplitude of injected current, which also typically causes the appearance of low-frequency spikes. As shown in Fig. 1(c), the response of CA1 neurons to a long positive-current injection exhibits rather regular spiking patterns with a slightly higher frequency of the spikes at the beginning of the stimulus (Andersen et al., 2007; Yue and Yaari, 2004; Yue et al., 2005; Yue and Yaari, 2006; Golomb et al., 2006; Yaari et al., 2007). In certain conditions, pyramidal cells produce series of bursts instead of tonic spiking; this behaviour is much more common for the CA3 pyramidal cells than the CA1 cells (Wong and Prince, 1981; Traub et al., 1991; Scharfman, 1993; Migliore et al., 1995; Safiulina et al., 2008; Brown and Randall, 2009). In CA1 neurons such bursting is usually related to abnormal conditions such as absence of Ca^{2+} in the bath solution (Yue and Yaari, 2004; Yue et al., 2005; Yue and Yaari, 2006; Golomb et al., 2006; Yaari et al., 2007).

A characteristic feature of the CA1 and CA3 area neurons that becomes evident during experiments is the so-called after-depolarisation (ADP), also known as depolarising afterpotential (DAP) (Wong and Prince, 1981; Izhikevich, 2006; Brown and Randall, 2009). It is a positive deflection of the membrane potential, which creates the characteristic 'hump' shown in Figs. 1 (b) and (d). The amplitude of the ADP is usually larger for the CA3 neurons (Wong and Prince, 1981; Andersen et al., 2007). Furthermore, ADP with sufficiently high amplitude produces a burst of several spikes in both CA1 and CA3 neurons (Wong and Prince, 1981; Yue and Yaari, 2004; Yue et al., 2005; Brown and Randall, 2009; Yaari et al., 2007). Due to its importance for neural excitability ADP has been the focus of many recent experimental studies (Yue and Yaari, 2004; Yue et al., 2005; Yue and Yaari, 2006; Golomb et al., 2006; Yaari et al., 2007; Chen and Yaari, 2008; Safiulina et al., 2008; Brown and Randall, 2009). It has been shown that this phenomenon is regulated by muscarinic-sensitive (M-type) K^{+}-channels (Yue and Yaari, 2004, 2006). More recent results also indicate that persistent Na^{+}-channels (Yue et al., 2005; Golomb et al., 2006) and transient Ca^{2+}-channels (Chen and Yaari, 2008) play an important role for ADP regulation. Furthermore, these studies suggest that ADP is an intrinsic feature of the pyramidal cells (Yue et al., 2005; Golomb et al., 2006; Yaari et al., 2007; Chen and Yaari, 2008; Safiulina et al., 2008; Brown and Randall, 2009). In this paper we present a modelling study of CA1/3 pyramidal cells focussing on how the intrinsic properties of the cell body (soma) shape the ADP. Accordingly, we use Hodgkin-Huxley formalism (Hodgkin and Huxley, 1952) and consider only a somatic compartment in our model.

The model is parametrised according to our recent published (Brown and Randall, 2009) and unpublished experimental data; a few values are also based on other published experimental measurements (Liu et al., 2003; Yue and Yaari, 2004, 2006; Yaari et al., 2007; Yue et al., 2005; Golomb et al., 2006; Blackmer et al., 2009; Destexhe and Bal, 2009). Despite the fact that our study focusses mainly on the transient behaviour of a pyramidal neuron, the responses of CA1 and CA3 pyramidal cells to both long and short stimuli are also reproduced well by our model. To demonstrate this, we validate our model against such experimental data. Moreover, we show that the transition between the two types of pyramidal cells in the model can be obtained by

changing only three maximal conductances.

Although ADP has been studied experimentally quite extensively, the mechanisms underlying this phenomenon have received little theoretical attention. In particular, to date, there have been no attempts to formalise ADP mathematically. Having constructed a model validated by recent experimental data, we use it to dissect the ADP. We analyse ADP from a mathematical point of view and investigate what the underlying mechanisms are. In addition, we investigate the bursting-threshold for a burst of action potentials riding on top of the ADP, which is fundamentally different from the spiking-threshold of a single action potential. This transient bursting behaviour is not only important during physiological responses of a pyramidal cell, but is also related to pathological conditions characterised by hyperexcitability in the hippocampus, such as epilepsy (Kile et al., 2008; Misra et al., 2008). Furthermore, recent in-vivo experiments indicate that bursting takes place in hippocampal place cells during spatial navigation (Harvey et al., 2009) and, thus, could be important for memory and learning.

We end this study with a sensitivity analysis of the model. We investigate the effect of changing the maximal values of current conductances, because they are most likely to vary among cells. This analysis allows us to make predictions about the role of isolated currents for the behaviour of the model. We show that a decrease of high-voltage-activated inward currents can increase excitability and that low-voltage-activated currents have a profound influence on ADP.

All numerical computations were done with XPP (Ermentrout, 2002). We used the package XPPy (Nowacki, 2010) to perform the XPP simulations in Python (Oliphant, 2007) and visualise the results in Python using Matplotlib (Hunter, 2007).

2 General single-compartment model for CA pyramidal neuron cells

In our model we only take into account fast-activating ionic currents that are known to contribute to ADP and affect the model behaviour over relatively short periods of time (up to 500 ms). The model consists of the following ionic currents: two Na^+-currents, one transient ($I_{\mathrm{Na_T}}$) and one persistent ($I_{\mathrm{Na_P}}$); two Ca^{2+}-currents, one T type ($I_{\mathrm{Ca_T}}$) and one high voltage activated ($I_{\mathrm{Ca_H}}$); and three K^+-currents, delayed rectifier ($I_{\mathrm{K_{DR}}}$), M type ($I_{\mathrm{K_M}}$), and leak (I_{L}). We use Hodgkin-Huxley formalism (Hodgkin and Huxley, 1952) to represent the rate of change of the membrane potential:

$$C\frac{dV}{dt} = -I_{\mathrm{Na_T}} - I_{\mathrm{Na_P}} - I_{\mathrm{Ca_T}} - I_{\mathrm{Ca_H}} - I_{\mathrm{K_{DR}}} - I_{\mathrm{K_M}} - I_L + I_{\mathrm{app}}, \tag{1}$$

where C is the membrane capacitance. The ionic currents are modelled as:

$$\begin{aligned}
I_{\mathrm{Na_T}} &= g_{\mathrm{Na_T}} m_{\mathrm{Na_T}}^3 h_{\mathrm{Na_T}} (V - E_{\mathrm{Na}}), \\
I_{\mathrm{Na_P}} &= g_{\mathrm{Na_P}} m_{\mathrm{Na_P}} (V - E_{\mathrm{Na}}), \\
I_{\mathrm{Ca_T}} &= g_{\mathrm{Ca_T}} m_{\mathrm{Ca_T}}^2 h_{\mathrm{Ca_T}} (V - E_{\mathrm{Ca}}), \\
I_{\mathrm{Ca_H}} &= g_{\mathrm{Ca_H}} m_{\mathrm{Ca_H}}^2 h_{\mathrm{Ca_H}} (V - E_{\mathrm{Ca}}), \\
I_{\mathrm{K_{DR}}} &= g_{\mathrm{K_{DR}}} m_{\mathrm{K_{DR}}} h_{\mathrm{K_{DR}}} (V - E_{\mathrm{K}}), \\
I_{\mathrm{K_M}} &= g_{\mathrm{K_M}} m_{\mathrm{K_M}} (V - E_{\mathrm{K}}), \\
I_{\mathrm{L}} &= g_{\mathrm{L}} (V - E_{\mathrm{L}}).
\end{aligned}$$

and the gating variables are of the form

$$\frac{dx}{dt} = \frac{x_\infty - x}{\tau_x}, \tag{2}$$

$$\text{with } x \in \{m_{\mathrm{Na_T}}, h_{\mathrm{Na_T}}, m_{\mathrm{Na_P}}, m_{\mathrm{Ca_T}}, h_{\mathrm{Ca_T}}, m_{\mathrm{Ca_H}}, h_{\mathrm{Ca_H}}, m_{\mathrm{K_{DR}}}, h_{\mathrm{K_{DR}}}, m_{\mathrm{K_M}}\}.$$

The activation and inactivation steady-state functions x_∞ of the respective currents are given in Boltzmann form:

$$x_\infty = \frac{1}{1 + \exp(-(V - V_x)/k_x)},$$

and the time scales τ_x are all constant, except for the transient Na^+-channel, namely,

$$\tau_{\mathrm{h_{Na_T}}}(V) = 0.2 + 0.007 \exp(\exp(-(V - 40.6)/51.4)), \tag{3}$$

is modeled as voltage dependent in order to obtain a better fit for our data.

The parameters of the pyramidal neuron model are given in Table 1. In the following section we validate our model against CA1 and CA3 current-clamp experiments by varying the maximal conductances (g_x). Therefore, these values are not included in Table 1, but given in Section 3. Most of the model parameters in Table 1 are determined by voltage-clamp experimental measurements (Liu et al., 2003; Yue and Yaari, 2004, 2006; Yaari et al., 2007; Yue et al., 2005; Golomb et al., 2006; Blackmer et al., 2009; Destexhe and Bal, 2009); an example is shown in Fig. 2(a) for the Na^+-current. Figures 2(a), (b) and (c) show the steady-state activation and inactivation functions $m_{\mathrm{Na_{T_\infty}}}$, $h_{\mathrm{Na_{T_\infty}}}$ and $m_{\mathrm{Na_{P_\infty}}}$ of the Na^+-channel currents, $m_{\mathrm{Ca_{T_\infty}}}$, $h_{\mathrm{Ca_{T_\infty}}}$, $m_{\mathrm{Ca_{H_\infty}}}$ and $h_{\mathrm{Ca_{H_\infty}}}$ of the Ca^{2+}-channel currents, and $m_{\mathrm{K_{DR_\infty}}}$, $h_{\mathrm{k_{DR_\infty}}}$ and $m_{\mathrm{K_{M_\infty}}}$ of the K^+-channel currents, respectively. The curve in Fig. 2(d) illustrates the behaviour of the time constant $\tau_{h_{\mathrm{Na_T}}}$ of the transient Na^+-channel.

3 Model validation

We validate the pyramidal neuron model by simulating experimental responses of a typical neuron cell from the CA1 and CA3 areas (see Fig. 1). The goal is to identify a set of maximal

Table 1: Parameter values of the pyramidal neuron model.

Parameter	Value	Unit	Parameter	Value	Unit
C_{m}	1	μF/cm^2	$\tau_{\mathrm{h}_{\mathrm{Ca_T}}}$	32	ms
E_{Na}	60	mV	$V_{\mathrm{m}_{\mathrm{Ca_H}}}$	-15	mV
E_{K}	-85	mV	$k_{\mathrm{m}_{\mathrm{Ca_H}}}$	5	mV
E_{Ca}	90	mV	$\tau_{\mathrm{m}_{\mathrm{Ca_H}}}$	0.08	ms
E_{L}	-65	mV	$V_{\mathrm{h}_{\mathrm{Ca_H}}}$	-60	mV
$V_{\mathrm{m}_{\mathrm{Na_T}}}$	-37	mV	$k_{\mathrm{h}_{\mathrm{Ca_H}}}$	-7	mV
$k_{\mathrm{m}_{\mathrm{Na_T}}}$	5	mV	$\tau_{\mathrm{h}_{\mathrm{Ca_H}}}$	300	ms
$V_{\mathrm{h}_{\mathrm{Na_T}}}$	-75	mV	$V_{\mathrm{m}_{\mathrm{K_{DR}}}}$	-5.8	mV
$k_{\mathrm{h}_{\mathrm{Na_T}}}$	-7	mV	$k_{\mathrm{m}_{\mathrm{K_{DR}}}}$	11.4	mV
$V_{\mathrm{m}_{\mathrm{Na_P}}}$	-47	mV	$\tau_{\mathrm{m}_{\mathrm{K_{DR}}}}$	1	ms
$k_{\mathrm{m}_{\mathrm{Na_P}}}$	3	mV	$V_{\mathrm{h}_{\mathrm{K_{DR}}}}$	-68	mV
$V_{\mathrm{m}_{\mathrm{Ca_T}}}$	-54	mV	$k_{\mathrm{h}_{\mathrm{K_{DR}}}}$	-9.7	mV
$k_{\mathrm{m}_{\mathrm{Ca_T}}}$	5	mV	$\tau_{\mathrm{h}_{\mathrm{K_{DR}}}}$	1400	ms
$\tau_{\mathrm{m}_{\mathrm{Ca_T}}}$	2	ms	$V_{\mathrm{m}_{\mathrm{K_M}}}$	-30	mV
$V_{\mathrm{h}_{\mathrm{Ca_T}}}$	-65	mV	$k_{\mathrm{m}_{\mathrm{K_M}}}$	10	mV
$k_{\mathrm{h}_{\mathrm{Ca_T}}}$	-8.5	mV	$\tau_{\mathrm{m}_{\mathrm{K_M}}}$	75	ms

conductances that reproduce an example of 'avarage' CA1 and CA3 pyramidal neurons. We compare model simulations to two major types of current-clamp experiments: short- and long-current stimuli. The long-stimulus experiment is the application of a current injection with a prespecified amplitude that lasts 500 ms. The amplitude is typically 100, 200 or 300 pA. The injection amplitudes in the model are then 1, 2, 3 $\mu\mathrm{A}/\mathrm{cm}^2$, respectively, because the model takes into account current densities and we simulate a whole-cell current-clamp experiment of a pyramidal neuron with a typical somatic capacitance between 90–120 pF (unpublished observations). In the short-stimulus experiment the current injection is applied for 2 ms and the amplitude is much larger, namely, 2 nA. In the model we set the amplitude of the applied current accordingly to 20 $\mu\mathrm{A}/\mathrm{cm}^2$. In some experiments the cell is made genotype independent by fixing its resting potential to a specific value that is slightly different from the physiological value (Brown and Randall, 2009). To achieve this, the cells are pre-stimulated with a steady-state current injection of an appropriate amplitude. In the model we set the resting potential to the required level by using a nonzero base value of the injected current.

In order to validate the model against the experimental results, we also compare a number of model-derived quantities that correspond to measured electrophysiological properties (Brown and Randall, 2009). These are the action-potential threshold, the membrane resting potential and the action-potential peak. As in (Brown and Randall, 2009) the evaluation of these quantities is done for a current injection of 300 pA, i.e., 3 $\mu\mathrm{A}/\mathrm{cm}^2$ in our model. For both CA1 and CA3 neurons the membrane resistance is the same and given by $R_{\mathrm{m}} = 50,000\ \Omega/\mathrm{cm}^2$. Therefore, with a membrane capacitance of 1 $\mu\mathrm{F}/\mathrm{cm}^2$, the membrane time constant is $\tau_m = 50$ ms. Note that this value is typically found experimentally for pyramidal cells (Brown and Randall, 2009).

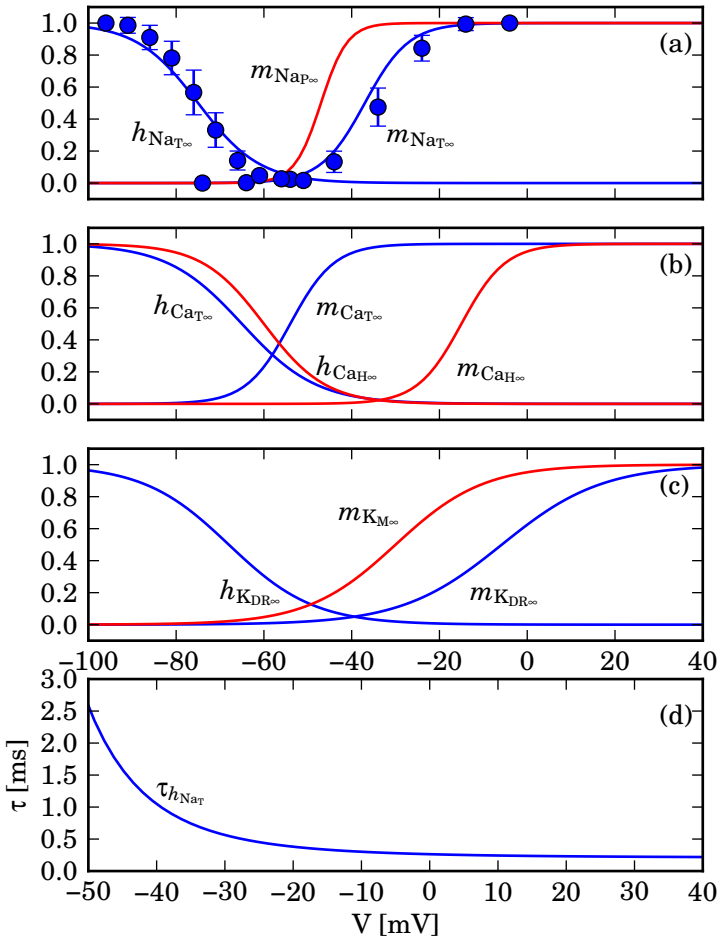

Figure 2: Channel kinetics used in the pyramidal neuron model; panels (a), (b) and (c) show (in)activation functions of Na^+-, Ca^{2+}- and K^+-channel currents, respectively; experimental measurements used to determine Na^+-current (in)activation parameters are depicted as blue dots in panel (a) with standard deviations marked by the error bars; panel (d) shows the time rate of the transient Na^+-channel.

Table 2: Maximal conductance values of the model of the CA3 area neuron.

Parameter	Value	Unit	Parameter	Value	Unit
$g_{\mathrm{Na_T}}$	65	mS/cm^2	$g_{\mathrm{K_{DR}}}$	10	mS/cm^2
$g_{\mathrm{Na_P}}$	0.1	mS/cm^2	$g_{\mathrm{K_M}}$	1.65	mS/cm^2
$g_{\mathrm{Ca_T}}$	0.74	mS/cm^2	g_{L}	0.02	mS/cm^2
$g_{\mathrm{Ca_H}}$	2.6	mS/cm^2			

3.1 Long-stimulus experiment

The model simulations for the CA3 neuron were performed with the values of the ionic-current kinetics given in Table 1 and the maximal conductances presented in Table 2. In Fig. 3 we

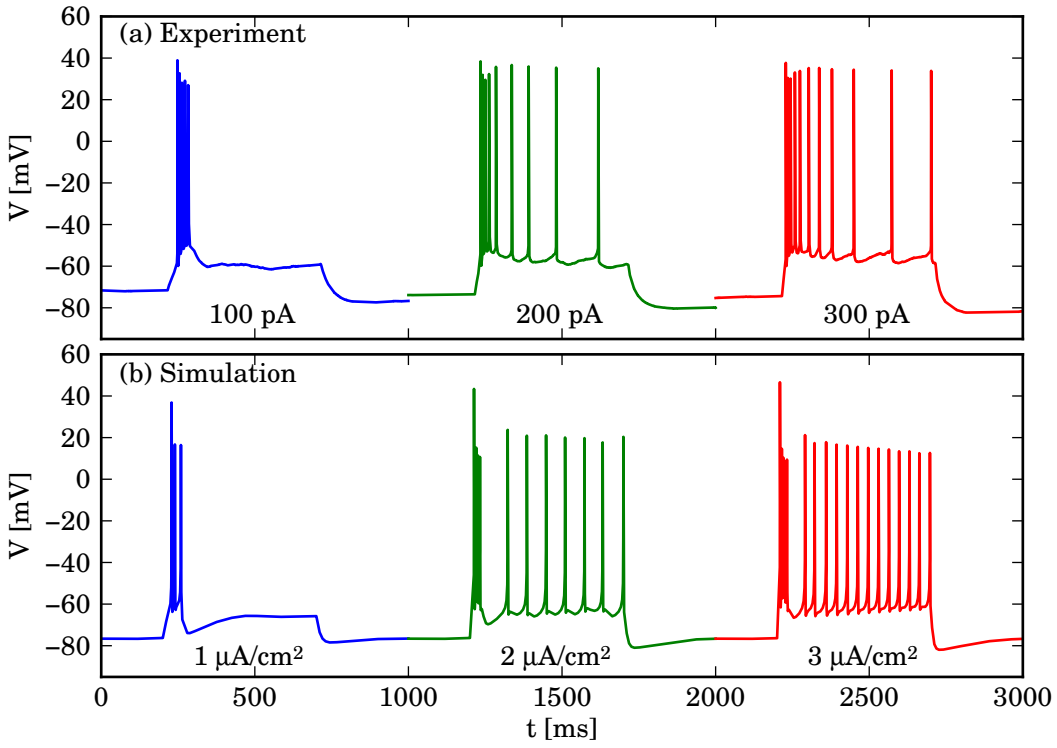

Figure 3: Responses of a CA3 pyramidal neuron and our model to a 500 ms current injection; panel (a) shows experimental responses of a pyramidal cell, where the injected current has amplitudes 100, 200 and 300 pA; panel (b) shows the corresponding responses of the model to 1, 2 and 3 $\mu\mathrm{A}/\mathrm{cm}^2$ of injected current.

illustrate experimental and simulation responses to 500 ms depolarising current injections. The time trace of the experimental membrane potential of a pyramidal neuron to injections of 100, 200 and 300 pA depolarising currents is shown in Fig. 3(a). The corresponding responses of the model to current injections of magnitudes 1, 2 and 3 $\mu\mathrm{A}/\mathrm{cm}^2$ are shown in Fig. 3(b). The resting potential for the model with the CA3 parameter set is -76.6 mV for all of the traces in Fig. 3(b). The action-potential peak for 3 μA/cm^2 current injection is 46.6 mV. The spike-threshold for the experimental and model responses due to highest current injection is approximately -58 mV as shown in Fig. 3(a) and (b). These values are within the interval of physiological responses (Andersen et al., 2007; Brown and Randall, 2009).

As depicted in Fig. 3 the overall responses of the model to the injected currents agrees with the experimental measurements, and is also in accordance with previously published results in (Andersen et al., 2007; Brown and Randall, 2009). For the lowest current injection of 1 $\mu\mathrm{A}/\mathrm{cm}^2$ only the initial high-frequency burst is produced, which is not followed by other additional spikes, as in Fig. 1(a). Higher-current injections produce a series of low-frequency action potentials. Also, the frequency and number of spikes increase with the amplitude of the injected current.

Next, we discuss the contribution and significance of each of the currents that are included in the model for reproducing the experimentally-observed CA3-pyramidal-cell behaviour. Transient Na^+-current is known to be responsible for the generation of action potentials (Hodgkin and Huxley, 1952). We chose the parameters for this current based on experimental studies performed at close-to-physiological temperatures of $33^\circ\mathrm{C}$ (Brown and Randall, 2009), with $m_{\mathrm{Na_{T\infty}}}$ and $h_{\mathrm{Na_{T\infty}}}$ as shown in Fig. 2(a). The activation of this channel is known to be sufficiently fast (Hodgkin and Huxley, 1952) (faster than the inactivation that is characterised by a minimal value of 0.2 ms; see Fig. 2(d)). Therefore, we neglect its dynamics and assume that it is instantaneous, i.e., $m_{\mathrm{Na_T}} = m_{\mathrm{Na_{T\infty}}}$. For values of the membrane potential that correspond to excitable behaviour, $\tau_{h_{\mathrm{Na_T}}}$ is below 1 ms, with a minimal value of 0.2 ms. Hence, inactivation is a relatively fast process that corresponds to the small region in Fig. 2(a) where $m_{\mathrm{Na_{T\infty}}}$ and $h_{\mathrm{Na_{T\infty}}}$ are both positive and only results in contributions from $I_{\mathrm{Na_T}}$ during the rising phase of the action potential. Because $I_{\mathrm{Na_T}}$ is so selective, we need to take into account an additional transient depolarising current, which is active in the low-voltage interval so that it influences the behaviour between the action potentials.

The persistent Na^+-current also plays an important role in the generation of action potentials (Yue et al., 2005; Golomb et al., 2006). The kinetics of this channel have been adopted from earlier modelling studies (Golomb et al., 2006). We note that they are also in accordance with recent dynamic-clamp experiments (Destexhe and Bal, 2009). Similar to the transient Na^+-channel, persistent Na^+-channel activation is known to be very fast (Golomb et al., 2006); hence, we again neglect its dynamics, i.e, $m_{\mathrm{Na_P}} = m_{\mathrm{Na_{P\infty}}}$. In addition, due to the steeper slope of $m_{\mathrm{Na_{P\infty}}}$ (see Fig. 2(a)), a small increase of the membrane potential is sufficient to activate $I_{\mathrm{Na_P}}$ fully. Note also that this current does not inactivate, which makes it an important determinant of the long-term behaviour of the membrane potential. The combination of low-voltage activation and persistence allows this current to contribute actively to the generation of action potentials for the duration of a simulation.

In addition to Na^+-channels, recent research shows that Ca^{2+}-channels are also actively involved in neural responses to stimuli (Yaari et al., 2007). Moreover, Ca^{2+}-channels are found to be present in both CA1 and CA3 pyramidal cells (Jaffe et al., 1994; Yaari et al., 2007). In our model we use two classes of Ca^{2+}-channels, low-voltage-activated T-type Ca^{2+}-channels and a general class of high-voltage-activated Ca^{2+}-channels. The kinetic parameters of a T-type Ca^{2+}-channel in our model are based on (Blackmer et al., 2009) and our data. To model this current, we use values similar to those published in (Jaffe et al., 1994; Migliore et al., 1995; Lazarewicz et al., 2002; Xu and Clancy, 2008). As shown in Fig. 2(b), the T-type Ca^{2+}-channel operates in the low-voltage interval and hence is an important building block of the neuron's ADP (Yaari et al., 2007). The steady-state inactivation function $h_{\mathrm{Ca_{T\infty}}}$ is quite close to $m_{\mathrm{Ca_{T\infty}}}$ and has a flat slope. As a result there is a large intersection area under the curves, that allows $I_{\mathrm{Ca_T}}$ to work for a larger range of low values of the membrane potential. In addition, the inactivation of $I_{\mathrm{Ca_T}}$ is a relatively slow process (see $\tau_{h_{\mathrm{Ca_T}}}$ in Table 1) that contributes to the transient excitability in the beginning of the current-injection stimulus. The main role of $I_{\mathrm{Ca_T}}$ in the model is to bring the membrane potential up, near the action-potential threshold, so that the other currents produce a spike. The high-voltage-activated Ca^{2+}-channel current plays a role in shaping the action potentials in our model. In particular, it determines their amplitudes. The gating parameters for this

channel are based on values in (Liu et al., 2003; Blackmer et al., 2009) and our data; their values are similar to those used in (Jaffe et al., 1994; Migliore et al., 1995; Lazarewicz et al., 2002; Xu and Clancy, 2008). Also note that the value of the time constant of $m_{\mathrm{Ca_H}}$ is low and it is one of the fastest currents in the model (see $\tau_{m_{\mathrm{Ca_H}}}$ in Table 1). To capture the effect of amplitude modulation observed in pyramidal cells, we allow $I_{\mathrm{Ca_H}}$ to inactivate. Note that this inactivation is a slow process (see $\tau_{h_{\mathrm{Ca_H}}}$ in Table 1), so that the inactivation of $I_{\mathrm{Ca_H}}$ is only significant for long spike-trains with a higher mean frequency.

The main outward current in our model is K^+ delayed rectifier, representing a number of fast K^+-currents. In our model K^+ delayed rectifier is a transient current, with a very slow inactivation. This slow inactivation is often neglected in models, because it hardly affects spiking. However, it plays an important role in setting the resting potential of the cell that corresponds to the initial conditions in the model.

It has been shown experimentally that the muscarinic-sensitive K^+-channel is important for the ADP of pyramidal cells (Yue and Yaari, 2004, 2006; Yaari et al., 2007). The parameters used in our model are based on (Oldfield et al., 2009). The muscarinic-sensitive K^+-current $I_{\mathrm{K_M}}$ does not inactivate (Yue and Yaari, 2004, 2006). Hence, it is active for a wide range of values of the membrane potential. Because $I_{\mathrm{K_M}}$ activates slowly, its contribution to the spike inhibition is lower at the beginning of the current injection. Hence, the lower initial inhibition allows for the forming of the characteristic transient burst in CA3 response (see Fig. 3).

Next, we demonstrate that our pyramidal-neuron model is capable of simulating CA1-area neural responses by changing three maximal conductance values, namely, $g_{\mathrm{Ca_T}} = 0.6$ mS/cm^2, $g_{\mathrm{K_{DR}}} = 9.5$ mS/cm^2 and $g_{\mathrm{K_M}} = 0.8$ mS/cm^2. The other values are as given in Tables 1 and 2. Such changes may reflect a difference in the number of ion channels among CA1 and CA3 neurons. The time trace of the experimental membrane-potential response of a pyramidal neuron to the injection of 100, 200 and 300 pA depolarising current is shown in Fig. 4(a). The corresponding responses of the model to the injection of 1, 2 and 3 $\mu\mathrm{A/cm}^2$ depolarising current is shown in Fig. 4(b). The membrane resting potential for the model with the CA1 parameter set is -75.5 mV for all of the traces in Fig. 4(a). Hence, the value is within the physiological range for this class of neurons (Golomb et al., 2006; Andersen et al., 2007; Yaari et al., 2007). The action-potential peak and threshold for 3 μA/cm^2 current injection are approximately 44.9 mV and -60 mV, respectively. This agrees with our experimental results and published data in (Golomb et al., 2006; Yaari et al., 2007).

As illustrated in Fig. 4, the overall response of the model to injected current agrees very well with the experimental data (Fig. 4(a)), and is also in accordance with previously published results (Golomb et al., 2006; Andersen et al., 2007; Yaari et al., 2007). The response is characterised by relatively regular long-term spike frequencies, with a slight increase just after the start of the current injection. Also, the frequency and number of spikes increase with the amplitude of the injected current. Note that, compared with the CA3 neural response (Fig. 3(a)), the number as well as the mean frequency of the action potentials is higher. Moreover, due to inactivation of $I_{\mathrm{Ca_H}}$ the characteristic modulation of the peaks of the action potential is captured in the response of the model. The gradual increase of the baseline is also reproduced well by the model. This phenomenon is caused by the inactivation of $I_{\mathrm{K_{DR}}}$.

Thus, our results suggest that the CA1 neuron may have slightly fewer transient Ca^{2+}-

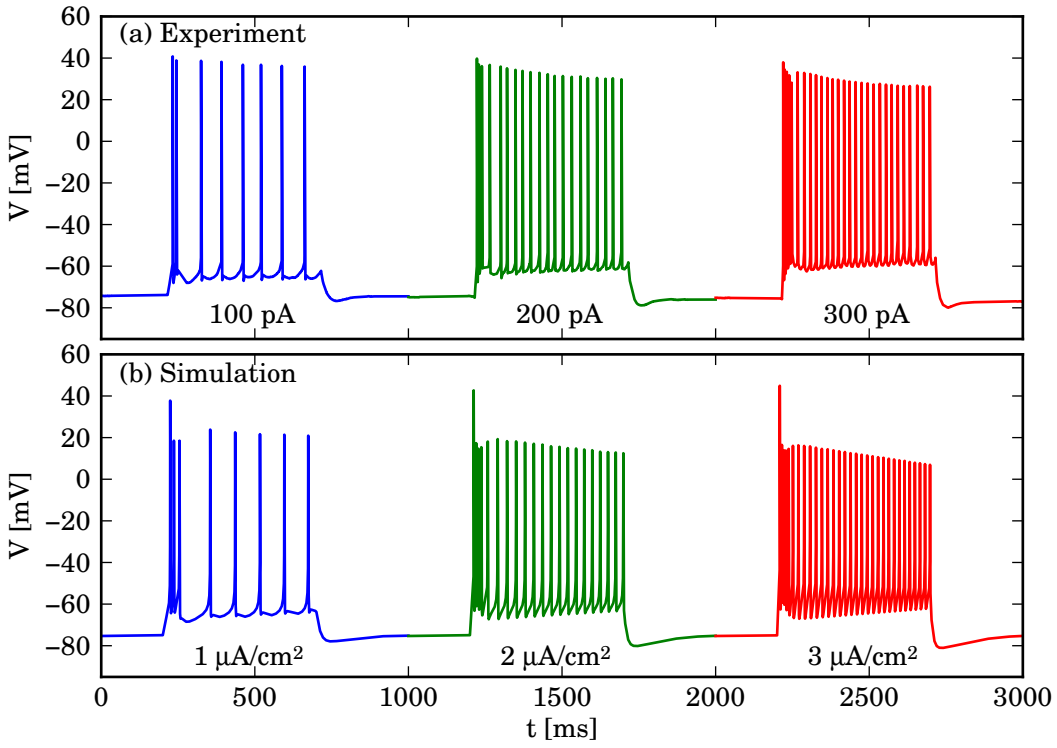

Figure 4: Responses of a CA1 pyramidal neuron and our model to a 500 ms current injection; panel (a) shows experimental responses of a pyramidal cell, where the injected current has amplitudes 100, 200 and 300 pA; panel (b) shows the corresponding responses of the model to 1, 2 and 3 $\mu\mathrm{A}/\mathrm{cm}^2$ of injected current.

channels and delayed rectifier K^+-channels, and far fewer M-type K^+-channels. This also emphasises the importance of M-type K^+-current for the long-term spiking behaviour and overall excitability as has been demonstrated experimentally in (Yue and Yaari, 2004, 2006; Yaari et al., 2007). Interestingly, model simulations (not shown) indicate that only decreasing the value of $g_{\mathrm{K_M}}$ for the CA3 neuron parameter set already rapidly increases the number and frequency of action potentials, which is a key feature of CA1-like behaviour.

3.2 Short-stimulus experiment

We now focus on the model response to a short current injection. In Fig. 5 we illustrate model simulations of 2 ms current injections of 20 $\mu\mathrm{A}/\mathrm{cm}^2$ with different (pre-stimulus) base currents that impose a pre-defined resting potential of the cell. The time traces of the membrane potential of the model with the CA3 parameter set and an injected current with base current values of 0, 0.4 and 0.8 μA/cm^2 are shown in Fig. 5(a). Similarly, the time traces of the membrane potential of the model with the CA1 parameter set and an injected current with base current values of 0, 0.2 and 0.4 μA/cm^2 are shown in Fig. 5(b). The simulated traces are overlaid to show how the

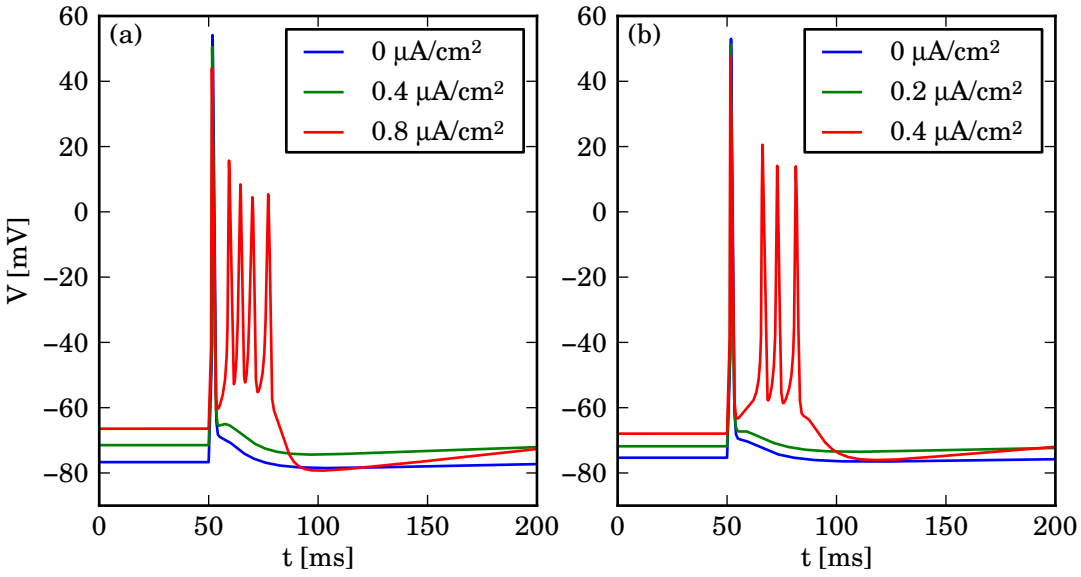

Figure 5: Responses of the pyramidal model neuron to the 2 ms current injection of 20 $\mu\mathrm{A}/\mathrm{cm}^2$; panel (a) shows overlaid responses of the model with the CA3 parameter set to a stimulus with different (pre-stimulating) base currents, namely, 0 $\mu\mathrm{A}/\mathrm{cm}^2$ (blue), 0.4 $\mu\mathrm{A}/\mathrm{cm}^2$ (green) and 0.8 $\mu\mathrm{A}/\mathrm{cm}^2$ (red); similarly, panel (b) shows overlaid responses of the model with the CA1 parameter set to a stimulus with different base currents, namely, 0 $\mu\mathrm{A}/\mathrm{cm}^2$ (blue), 0.2 $\mu\mathrm{A}/\mathrm{cm}^2$ (green) and 0.4 $\mu\mathrm{A}/\mathrm{cm}^2$ (red);

after-depolarisation grows with the changes in the membrane resting potential.

Figure 5 illustrates that the model is capable of simulating the experimental results shown in Figs. 1(b) and (d) and in (Brown and Randall, 2009; Golomb et al., 2006; Andersen et al., 2007; Yaari et al., 2007), including the characteristic shape of the after-depolarisation 'hump'. Moreover, as reported in (Golomb et al., 2006; Brown and Randall, 2009), as soon as the membrane resting potential exceeds approximately -70 mV, a burst of action potentials is produced, which is clearly illustrated by the last (highest) trace in Figs. 5(a) and (b). Although the shape of the after-depolarisation is reproduced quite well, the duration of the simulated after-depolarisation is slightly shorter than for the experimental measurements. The main reason for this difference is the fact that we use constant values for the time constants of most of the currents; in real cells these are most likely voltage dependent. Compared to the simulations of the model with the CA3 parameter set in Fig. 5(a), the amplitude of ADP for the CA1 model is noticeably smaller, which agrees well with experimental observations (Golomb et al., 2006; Andersen et al., 2007; Yaari et al., 2007). The reduction in amplitude of ADP is due to the smaller value of $g_{\mathrm{Ca_T}}$ in the CA1 parameter set. This causes less inward current to be present in the low-voltage region, and, thus, the model ADP has a smaller amplitude, despite lower inhibition. This observation also supports the importance of $I_{\mathrm{Ca_T}}$ in ADP modulation.

4 Identification of after-depolarisation and the initial burst

In the previous section we validated the pyramidal neuron model against a wide range of excitable behaviours, including ADP, for a typical average neuron from regions CA1 and CA3. In this section we investigate the mechanisms that shape the ADP and the transient burst. As a starting point we formulate a mathematical definition of ADP in order to identify the roles of the ionic currents for ADP generation and modulation in the model. Finally, we discuss the connection between the ADP and transient bursts in the long-stimulus experiment.

4.1 Mathematical formulation of after-depolarisation

Although the phenomenon of ADP has been investigated experimentally for a number of years and its significance for neural excitability has been recognised, there have not been any attempts to formalise this behaviour. Generally ADP is defined as a positive deflection of the membrane potential immediately after an action potential (Izhikevich, 2006).

The ADP is a relatively slow transient process, that takes place below the spiking threshold of the pyramidal neuron as shown in the previous sections. Hence, the absolute value of the derivative dV/dt of the membrane potential should be below threshold. According to (Naundorf et al., 2006) an action potential occurs when dV/dt exceeds $20\mathrm{V/s}$. Hence, during ADP we require:

$$\frac{dV}{dt} < 20\ [\mathrm{V/s}]. \tag{4}$$

The positive deflection of the membrane potential, as observed in the time trace in Figs. 3(a) and 4(a), is characterised by a local minimum B at a time $t = t_{\mathrm{B}} > 0$ and a local maximum P for some $t = t_{\mathrm{P}} > t_{\mathrm{B}}$ of V, which define the beginning and the peak of the ADP, respectively. Hence, B and P satisfy:

$$\frac{dV}{dt}(t_{\mathrm{B}}) = 0 \quad \text{and} \quad \frac{d^2V}{dt^2}(t_{\mathrm{B}}) > 0, \tag{5}$$

$$\frac{dV}{dt}(t_{\mathrm{P}}) = 0 \quad \text{and} \quad \frac{d^2V}{dt^2}(t_{\mathrm{P}}) < 0, \tag{6}$$

such that $dV/dt \geq 0$ in the time interval $(t_{\mathrm{B}}, t_{\mathrm{P}})$. We use (4) to distinguish ADP from a genuine action potential by imposing the following constraint:

$$\frac{dV}{dt}(t) < 20, \text{ for all } t_{\mathrm{B}} \leq t \leq t_{\mathrm{P}}.$$

Figure 6 depicts analysis of ADP for a model simulation and an example of experimental measurements. In the model simulation the holding current was set to $0.4\ \mu\mathrm{A/cm^2}$ to pre-define a resting potential of approximately -72 mV, as was done in the experiments. The time traces shown in Figs. 6(a) and (b) represent the model simulation and experimental data, respectively. We use finite-difference approximation to estimate dV/dt numerically. For better comparison,

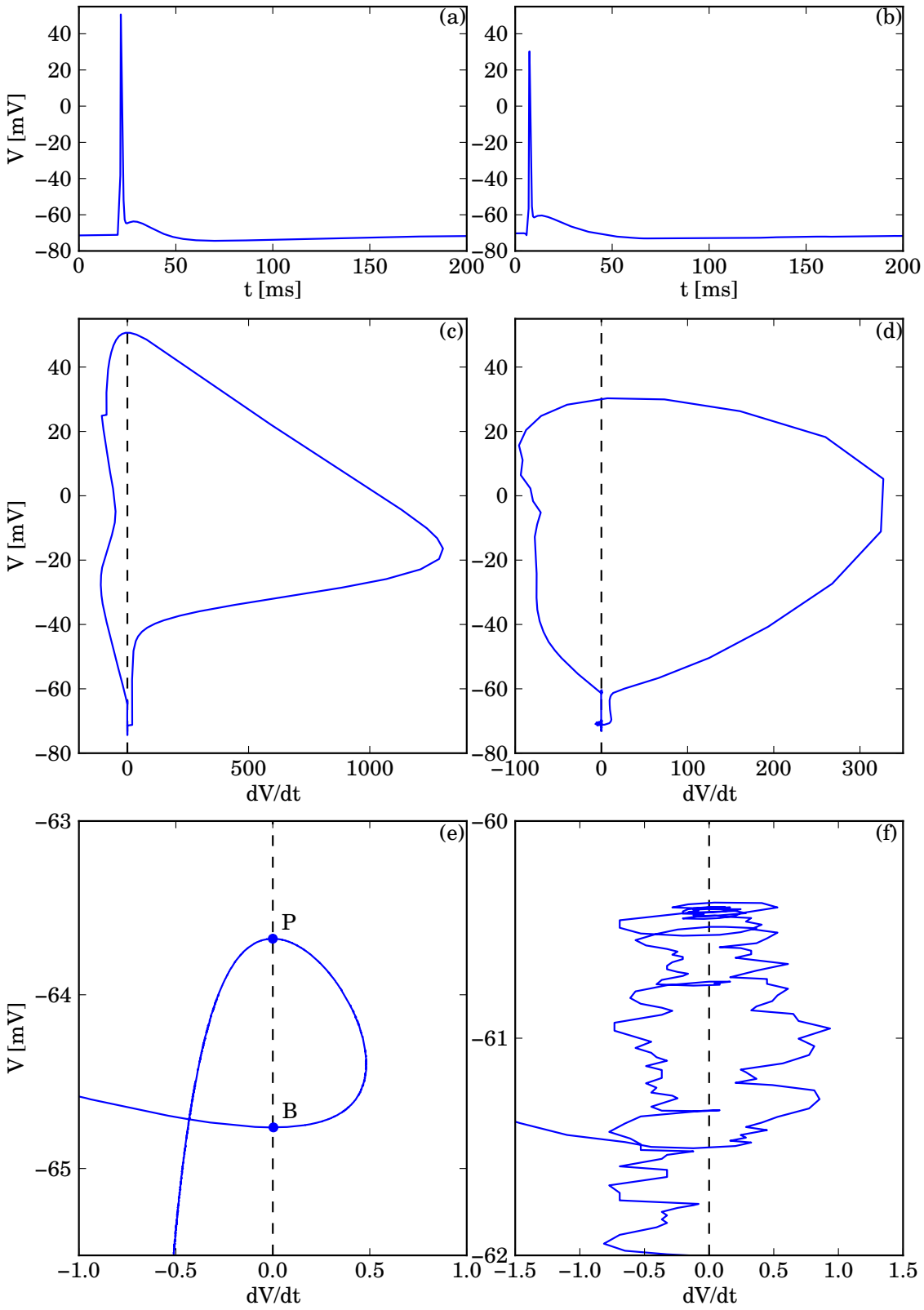

Figure 6: ADP in a CA3 pyramidal neuron for the model (first column) and the experiment (second column); panel (a) shows the time series of V for the model with a holding current of $0.4\ \mu\mathrm{A/cm^2}$; panel (b) shows the time series of V for an experimental sweep; panels (c) and (d) show the membrane potential V versus dV/dt; the dashed line marks $dV/dt = 0$; panels (e) and (f) show an enlargement of the ADP region, with the beginning B and peak P of the ADP marked for the model in panel (e).

we used the same approximation method for both data sets, because we did not observe a significant difference when deriving the values of dV/dt directly from the model equations. We used three-point simple moving average (mean) to smooth the experimental data. Further, more sophisticated processing of experimental measurements could be beneficial when the ADP is small. Figures 6 (c) and (d) show V versus dV/dt for the simulation and experiment, respectively. The vertical dashed line denotes the nullcline $dV/dt = 0$. The large excursions in Figs. 6(c) and (d) correspond to the action potentials generated by the current injection in the model and experiment, respectively. Although the shape of the derivative plot from our model simulation agrees with the experimental data, the maximum derivative is much higher compared to the experimental data. This is due to the assumption that the kinetics of Na^+ currents are instantaneous, which imposes an almost instantaneous growth of the action potential that results in an arbitrarily large derivative. The ADP itself is a much slower process, which takes place in the enlarged region shown in Figs. 6(e) and (f); the beginning point B and the peak value P of ADP for the model are marked on panel (e), but the ADP loop is also clearly visible in panel (f), despite the presence of noise for the experimental data. After the trajectory crosses the V-nullcline at B, which marks the beginning of ADP, the voltage V grows until the trajectory crosses the V-nullcline for a second time at P, which marks the peak of ADP. Note that dV/dt remains well below its threshold value of 20 V/s. The maximal value of dV/dt satisfies $d^2V/dt^2 = 0$ and corresponds to the point where ADP turns back toward the V-nullcline, while dV/dt remains positive.

The ADP takes place as soon as there are two local subthreshold extrema of the membrane potential. Therefore, the onset of ADP is the degenerate case where the trajectory develops a cubic tangency. Effectively, B and P coincide so that there exist a time t_{BP} after the action potential such that

$$\frac{dV}{dt}(t_{BP}) = 0 \quad \text{and} \quad \frac{d^2V}{dt^2}(t_{BP}) = 0, \tag{7}$$

that is, in the projection of V versus dV/dt, the trajectory is tangent to the V-nullcline (we assume that $d^3V/dt^3(t_{BP}) \neq 0$). The onset of ADP can be very hard to determine using just time series, whereas the derivative plot does this unmistakeably both for the simulations and the experimental measurements. Moreover, we can identify ADP-like behaviour, where dV/dt in the peak of the deflection is very close to V-nullcline, but dV/dt is negative. Such ADP-like behaviour can be deceiving when observing the time-trace plot, but it is readily distinguishable from ADP when determined by the derivative analysis.

Using the above approach we can also identify the underlying causes for generation of a burst riding on top of ADP, as presented in Fig. 5. Following condition (4), the action potential is generated when $dV/dt > 20$ at a time after the trajectory crosses the V-nullcline. Hence, dV/dt has to exceed the threshold value before reaching the turning point with $d^2V/dt^2 = 0$. Figure 7 illustrates this by plotting two trajectories, one with a single (blue) and one with an additional (green) action potential. Panel (a) shows the trajectory segments in the ADP region projected in $(d^2V/dt^2, dV/dt, V)$-space. The points where the segments intersect the planes $dV/dt = 0$ (cyan) and $d^2V/dt^2 = 0$ (red), that is, the V- and dV/dt-nullclines, are marked by dots and stars, respectively. Panel (b) provides a top view of panel (a); the trajectory segments are shown in projection onto the $(dV/dt, d^2V/dt^2)$-plane and the dashed lines correspond to the projections of

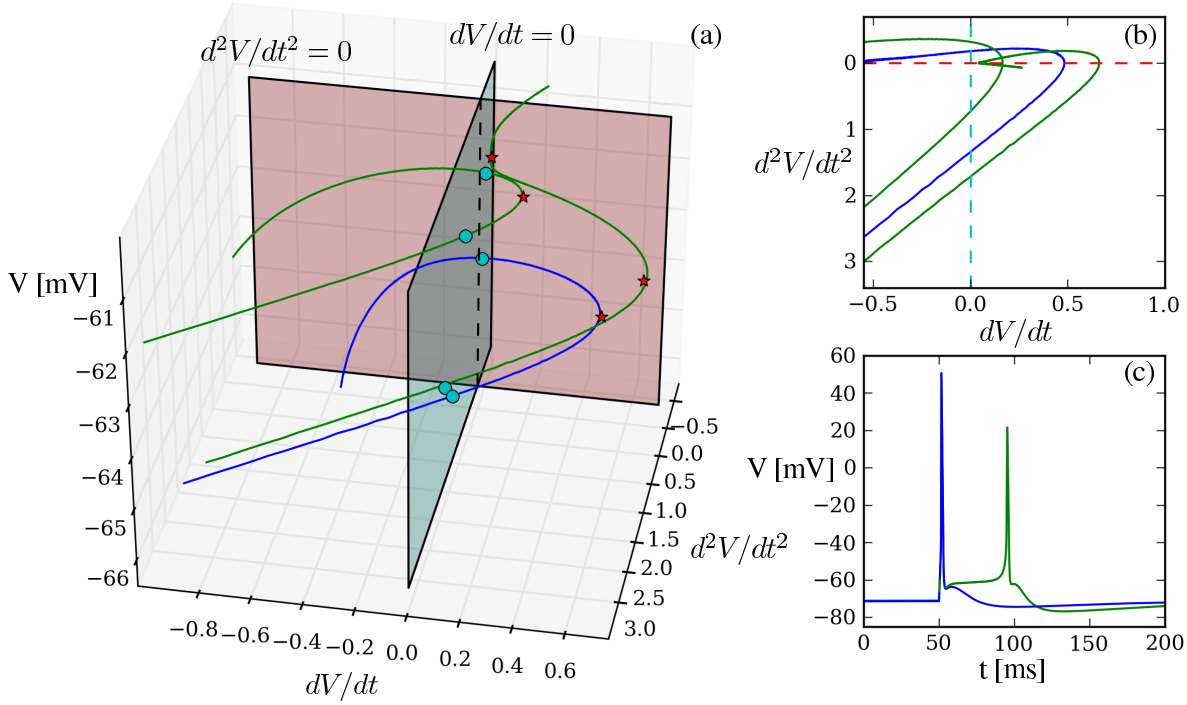

Figure 7: Bursting-threshold of the pyramidal neuron model; panel (a) shows trajectory segments of ADP without (blue) and with (green) a secondary spike in $(d^2V/dt^2, dV/dt, V)$-space; the intersections of the trajectory segments with the planes $dV/dt = 0$ (cyan) and $d^2V/dt^2 = 0$ (red) are marked by dots and stars, respectively; panel (b) presents a top view, namely, the projection onto the $(dV/dt, d^2V/dt^2)$-plane, with the projections of $dV/dt = 0$ (cyan) and $d^2V/dt^2 = 0$ (red) represented by dashed lines; panel (c) shows the time traces of the two trajectories.

the V- and dV/dt-nullclines. Note that d^2V/dt^2-axis in Fig. 7(b) is inverted to match Fig. 7(a). The time series of the trajectories for the two cases are shown in panel (c). The first (blue) trajectory in Fig. 7(a) is the same as the one in Fig. 6(e). After crossing the dV/dt-nullcline (red plane), the trajectory turns back to the V-nullcline (cyan plane), which marks the peak of ADP and results in a decrease of V. The burst trajectory (green) consists of two segments in Fig. 7(a); the s-shaped segment corresponds to the action-potential generation on top of the ADP, and the additional loop is the small 'hump' after the second spike (see Fig. 7(c)). The s-shaped trajectory also crosses the dV/dt-nullcline, i.e., $d^2V/dt^2 = 0$, and turns back toward the V-nullcline. However, before reaching the V-nullcline, it crosses the dV/dt-nullcline again. Thus, after the second crossing, dV/dt remains positive and an action potential is generated. Note that the burst trajectory is placed higher in V than the ADP trajectory. Moreover, the value of dV/dt before an action potential is fired in the burst case is larger than before the following 'hump'. Hence, the dV/dt-nullcline plays the role of a bursting-threshold in our model. Our study shows that as soon as a trajectory crosses the V-nullcline for the second time, no additional spikes will be generated.

4.2 The role of different ionic currents in shaping the after-depolarisation

In the previous section we defined the ADP phenomenon using the first and second derivatives of the membrane potential. We can use this information to determine the contribution of particular currents to the ADP. Both T-type Ca^{2+}-channel currents and persistent Na^{+}-channel currents are

known to facilitate ADP (Yue et al., 2005; Golomb et al., 2006; Chen and Yaari, 2008). The M-type K^+-channel current also mediates this phenomenon and is known to work for low values of the membrane potential (Yue and Yaari, 2004, 2006). Since the ADP is a low-voltage phenomenon, the main currents that play a role in its generation are low-voltage activated. Moreover, the ADP process is relatively slow in comparison to the spike-generation process; see Fig. 6 and also the time traces in Fig. 5. Hence, the currents that mediate ADP should be slower than the currents taking part in the process of spike generation.

In our model there are only four currents satisfying this condition, namely, $I_{\mathrm{Na_P}}$, $I_{\mathrm{Ca_T}}$, $I_{\mathrm{K_{DR}}}$ and $I_{\mathrm{K_M}}$. Note that only these four currents are active in the low-voltage region; the remaining currents are deactivated and effectively equal to zero. In addition, in our model $I_{\mathrm{Na_P}}$ in this region is small compared to the other participating currents. As illustrated in Fig. 6, $dV/dt < 0$ for most of the time after the action potential, because the membrane potential tries to return to its equilibrium (i.e. the resting potential). In order to create a time interval $(t_{\mathrm{B}}, t_{\mathrm{P}})$ during which $dV/dt > 0$, the total inward current must be larger than the total outward current. For low voltages in our model the total inward current is given by the sum of $I_{\mathrm{Na_P}}$ and $I_{\mathrm{Ca_T}}$, and the total outward current is the sum of $I_{\mathrm{K_{DR}}}$ and $I_{\mathrm{K_M}}$. Therefore, ADP is possible only if an interval $(t_{\mathrm{B}}, t_{\mathrm{P}})$ exists such that

$$I_{\mathrm{Na_P}}(t) + I_{\mathrm{Ca_T}}(t) > I_{\mathrm{K_{DR}}}(t) + I_{\mathrm{K_M}}(t), \quad t_{\mathrm{B}} \le t \le t_{\mathrm{P}}. \tag{8}$$

Condition (8) can be satisfied when there is a difference in the time scales of the currents participating in the ADP. The gating variable $m_{\mathrm{K_{DR}}}$ deactivates rapidly, which causes a reduction of the total outward current just after the action potential. Since $I_{\mathrm{Ca_T}}$ is the largest inward current, it mainly regulates the amount of the total inward current in the low-voltage area. The activation variable $m_{\mathrm{Ca_T}}$ of $I_{\mathrm{Ca_T}}$ has a slightly larger time constant than $m_{\mathrm{K_{DR}}}$ (see Table 1). Thus, its deactivation evolves slower than the deactivation of $I_{\mathrm{K_{DR}}}$, which allows the inward current to grow larger than the total outward current. Hence, there exists a period of time where the rate of change of the membrane potential is dominated by $I_{\mathrm{Ca_T}}$. This results in a positive sign of dV/dt and the membrane potential increases during this period. The slowest current involved in the ADP, namely, $I_{\mathrm{K_M}}$ mainly controls the duration of this phenomenon.

As shown in Fig. 5, a sufficiently high base-current injection can result in a burst on top of ADP. In general, ADP is generated by a perturbation in the membrane potential caused by a current injection. Therefore, after the first spike, the cell gradually returns to its resting state. Moreover, all currents evolve on their characteristic time scales, which causes the change in the sign of dV/dt. Nevertheless, not all currents activate during ADP. Only when the differences between the currents are sufficiently large and the membrane potential reaches larger values of V, can the Na^+-currents be activated. The second turn in Fig. 7 is caused by this gradual activation of Na^+-currents, which takes place around -60 mV (see Fig. 2(a)). The activation of additional inward currents cause dV/dt to increase and eventually generate an additional action potential on top of ADP, as shown in Figs. 5 and 7.

4.3 The after-depolarisation as a hallmark of CA1/3 neural excitability

Recent experimental studies (Golomb et al., 2006; Yaari et al., 2007; Brown and Randall, 2009) suggest that there is a direct relationship between ADP and excitability of pyramidal neurons. In this section we discuss why ADP is a hallmark of the excitability based on our modelling and experimental results. Since the behaviour of dV/dt, is determined by the dynamic interactions between the ionic currents in the system, we are able to define ADP in terms of the subthreshold difference of the ionic currents in the neuron. Figure 5(a) shows that a prominent ADP for the CA3 neuron causes the firing of a high-frequency transient burst. In contrast, CA1 neural response is characterised by a lower ADP, as illustrated in Fig. 5(b), and the transient burst has a lower frequency. We can explain this in terms of the amount of inward current that is active in the low-voltage region. Thus, more prominent ADP increases the probability of firing an action potential. It also marks a smaller initial inhibition by the outward currents, which allows the trajectory to reach the threshold faster and, hence, to produce a higher-frequency burst.

In our model the currents $I_{\mathrm{Na_P}}$, $I_{\mathrm{Ca_T}}$, $I_{\mathrm{K_{DR}}}$ and $I_{\mathrm{K_M}}$ that mediate ADP are also important for the generation of the action potentials. Since they work in the low-voltage region close to the spiking-threshold, they mainly regulate the probability of firing an action potential. Therefore, any change to those currents directly influences both ADP and overall excitability. Moreover, if the difference between the inward and outward currents is sufficiently large to bring the membrane potential to a value where Na^+-currents are engaged (around -60 mV in our model) additional spikes riding on top of the ADP are fired.

It is important to note that we investigate excitable behaviour in the model as part of the initial transient burst. Indeed, the initial response seems to be very important, because the stimuli during physiological conditions are more likely to be short, such as synaptic inputs. The above results indicate a direct connection between ADP and excitability, and suggest that CA3 neurons are more excitable than CA1 neurons as far as the transient burst is concerned. However, after the transient burst the CA1 neural response has much higher frequency and a larger number of spikes than the CA3 response. This behaviour in the model is caused by the different values of the $I_{\mathrm{K_M}}$ conductance $g_{\mathrm{K_M}}$. Finally, we observe a quite significant effect on the resting potential of the model neuron due to changes in $g_{\mathrm{K_{DR}}}$. This also influences the excitability through $h_{\mathrm{K_{DR}}}$, that limits the amount of active $I_{\mathrm{K_{DR}}}$ during the spike-train. Therefore, during the short-term stimulation there is effectively less $I_{\mathrm{K_{DR}}}$, so that the inward currents are less inhibited and action potentials will more likely be fired.

5 Parameter sensitivity analysis of the pyramidal neuron model

Parameter sensitivity analysis is a necessary step towards a better understanding of the model. It allows the investigation of the influence that particular parameter variations have on the behaviour of the system. Parameter sensitivity analysis also provides predictions that can be tested in further experimental studies of pyramidal neurons. In Section 3 we validated the model against a typical response of CA1 and CA3 neurons, whereas experiments show that the responses of the pyramidal neurons are much more versatile. We present a sensitivity analysis of our pyramidal

neuron based on what we call the excitability measure. In the subsequent sections we investigate the influence of all maximal conductances for the Na^+-, Ca^{2+}- and K^+-currents on the excitability behaviour of the model.

5.1 Methods

One of the most widely used measures for neural excitability is the so called mean instantaneous frequency for the number of first spike pairs. A characteristic feature of the pyramidal neuron response to long-current injection is a higher frequency of the first spike pairs. In order to capture this feature we define the excitability measure:

$$M_{\mathrm{e}} = \sum_{i=1}^{n} \frac{1}{i^2 (ISI)_i},$$

as a form of mean instantaneous frequency where the frequency of the initial spike pairs have larger weight. Here, n is the total number of spike pairs in an $(n+1)$-spike response and $(ISI)_i$ is the inter-spike interval of the pair i. The pair number is squared to increase the importance of the initial spike-pairs, because the frequency equilibrates rather fast. Note that the total number of spikes changes the (minimal) excitability measure. Hence, for a better comparison, we calculate this value for a constant number of spikes in a spike-train.

It is important to note that the parameters of the gating variables in our model are based on voltage-clamp experimental data and are measured with a high level of confidence. On the other hand voltage clamp allows to measure conductances that are present only on a patch of the neuron's membrane. Since we simulate whole-cell current-clamp recordings, the values of maximal conductances for such simulations are not very well defined. Therefore, we perform a sensitivity analysis with respect to the maximal conductances. They are also most likely to vary between the cells. In our analysis we vary only one conductance and keep the others at their reference values given in Tables 1 and 2. We use a $1\ \mu\mathrm{A/cm^2}$ current injection of duration 500 ms, which corresponds to the 100 pA injection in the experiment. This value was chosen because the pyramidal cells are reported to express more variability in behaviour under low-current injection (unpublished observations). We found that the outcome of the analysis is similar for both types of model CA1 and CA3 neurons, and chose to present the results for CA1 neurons only.

5.2 The Na^+-channel currents

Firstly, we investigate the influence of Na^+-currents on the excitability of our pyramidal neuron model. Figure 8 shows the excitability measure computed as functions of $g_{\mathrm{Na_T}}$ and $g_{\mathrm{Na_P}}$, shown in panels (a) and (c), respectively. The number of spikes corresponding to the values of $g_{\mathrm{Na_T}}$ and of $g_{\mathrm{Na_P}}$ are depicted in Figs. 8(b) and (d), respectively.

Counter-intuitively, the increase of $g_{\mathrm{Na_T}}$ results in a decrease of both the excitability measure and the number of spikes (Fig. 8(a) and (b)). This could be explained by the fact that $I_{\mathrm{Na_T}}$ mainly influences the amplitude of the action potentials and, hence, activates more outward currents.

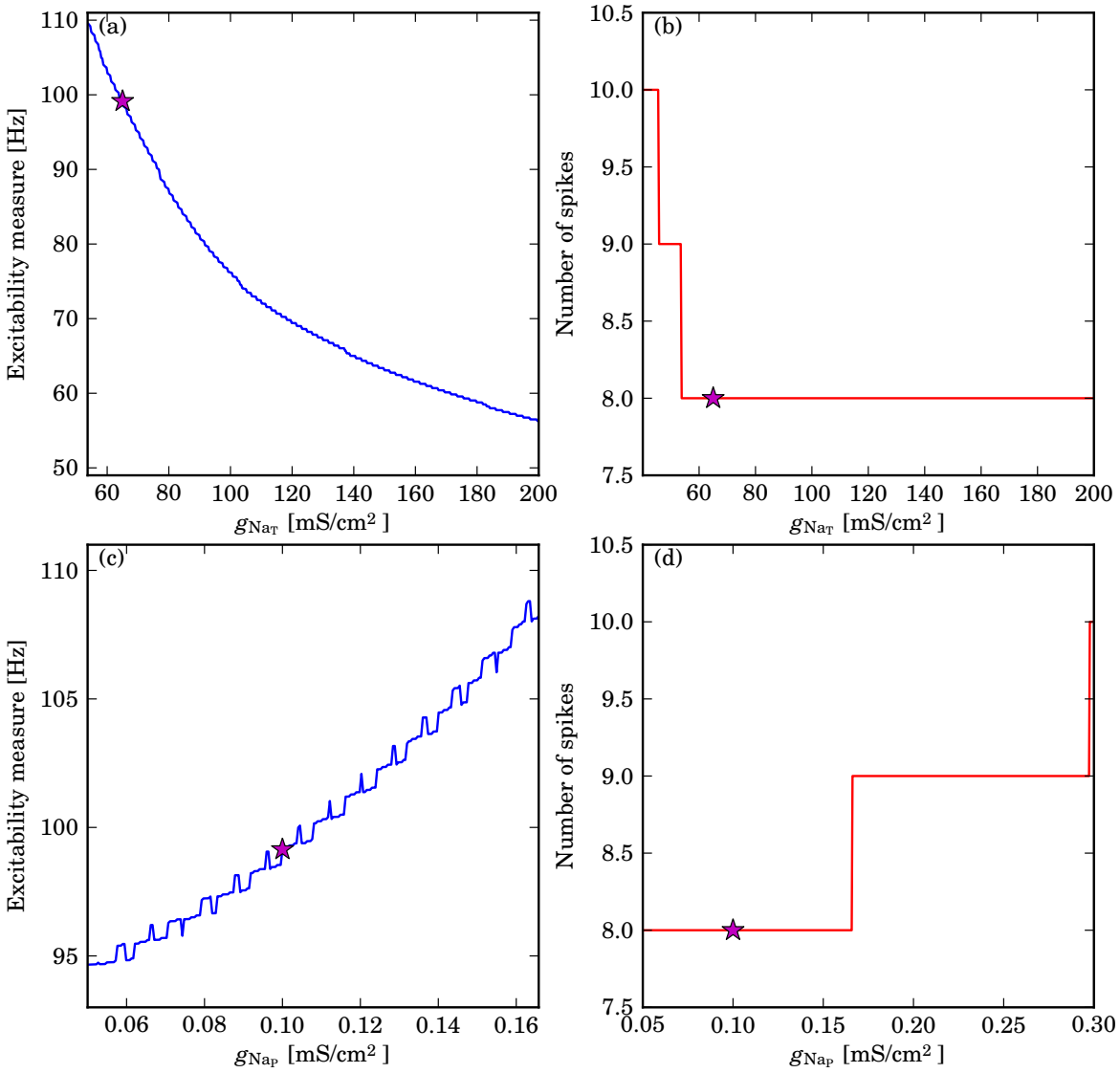

Figure 8: Parameter sensitivity analysis of the maximal conductances of the Na^+-currents; panels (a) and (c) show the excitability measure for ranges of $g_{\mathrm{Na_T}}$ and $g_{\mathrm{Na_P}}$, respectively; panels (b) and (d) show the numbers of spikes in a spike train for $g_{\mathrm{Na_T}}$ and $g_{\mathrm{Na_P}}$, respectively; the original values of the maximal conductances are marked by a (magenta) star.

Therefore, in contrast to what one would expect, excitability is indirectly inhibited by an increase of $g_{\mathrm{Na_T}}$. On the other hand, a decrease of $g_{\mathrm{Na_T}}$ causes an increase in the excitability, as a result of the lower inhibition of outward currents. Since $g_{\mathrm{Na_T}}$ is the same for CA1 and CA3 neurons in our model, the changes in this parameter have the same effect for both classes.

The influence of $g_{\mathrm{Na_P}}$ on the excitability of the model is more in line with intuition. As shown in Fig. 8(c) the increase in $I_{\mathrm{Na_P}}$ produces higher-frequency action potentials. Note that the value of the frequency measure is much larger than for $g_{\mathrm{Na_T}}$. On the other hand, $g_{\mathrm{Na_P}}$ has little influence on the number of spikes, as illustrated in Fig. 8(d), which reflects the low-voltage activation of this current. As shown above, it contributes to ADP and shapes the subthreshold behaviour of

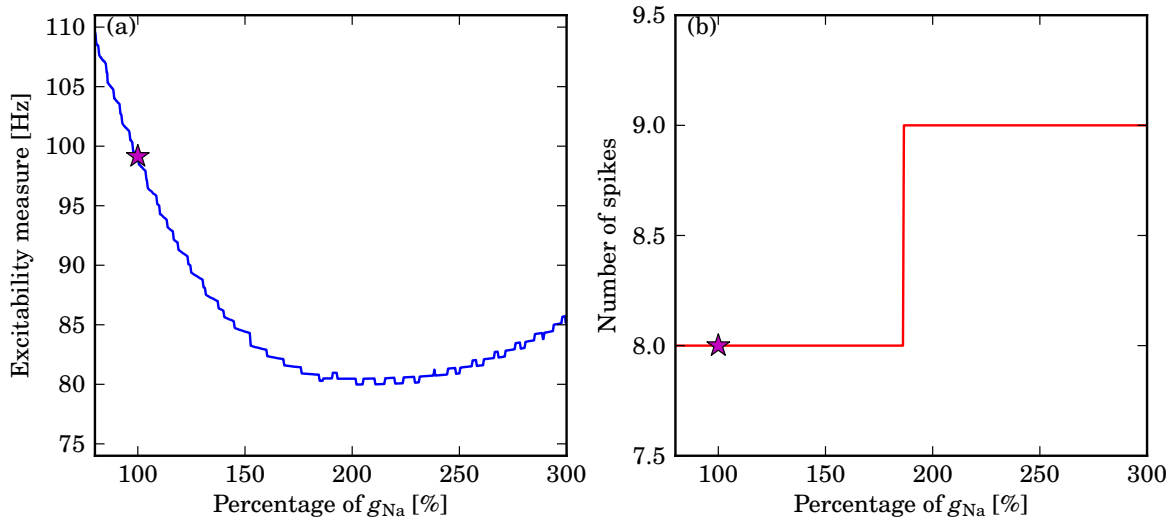

Figure 9: Parameter sensitivity analysis of the maximal conductance of the combined Na^+-currents; panel (a) shows the excitability measure ranging over the given percentages of g_{Na}; the original value of the maximal conductance is marked by a (magenta) star.

the derivative of the membrane potential, which is crucial for the action-potential generation. Note also that very small changes of $g_{\mathrm{Na_P}}$, compared to $g_{\mathrm{Na_T}}$, increase the value of the excitability measure quite dramatically. Despite the fact that the value of $g_{\mathrm{Na_P}}$ in our model is the same for both the CA1 and CA3 parameter sets, the high sensitivity to changes in this parameter can induce the variability of the neurons' responses reported in the experimental studies of mainly CA3 pyramidal cells (Wong and Prince, 1981; Traub et al., 1991; Scharfman, 1993; Migliore et al., 1995; Safiulina et al., 2008; Brown and Randall, 2009).

Due to a lack of pharmacological tools to influence $I_{\mathrm{Na_P}}$ selectively it is very hard to separate this current experimentally from the total Na^+-current recordings (Destexhe and Bal, 2009). Therefore, in order to compare with experimental data, we investigate the influence of both currents on the excitability. For this purpose we use a common parameter that modifies the percentages of $g_{\mathrm{Na_T}}$ and $g_{\mathrm{Na_P}}$ that are active in a given simulation run by the same factor. Here, the values from the CA1 set are used as the reference values. As before, the excitability measure and the number of spikes are plotted versus the percentage of total I_{Na} in Figs. 9(a) and (b), respectively. The effect of simulated change in both Na^+-currents produces a parabola-like characteristic curve in Fig. 9(a). It clearly illustrates that either an increase or decrease of I_{Na} can result in an increase of our neural excitability measure. In the studied interval, the increase of I_{Na} changes the number of spikes from eleven to ten, as shown in Fig. 9(b). Thus, our result suggests that there exists a minimum I_{Na} for which any perturbation of the Na^+-current could cause an increase in excitability. The analysis also shows how two different parameters that produce opposite excitability effects can cross-influence the response of a neuron. Moreover, it demonstrates how the total ionic current of a particular type can alter a pyramidal cell behaviour.

We observe this effect for CA3 parameter set as well. The minimum of excitability is reached, however, for greater percentage value of the total g_{Na}. This may be caused by the fact that the CA3 neuron model has a larger value of $g_{\mathrm{K_M}}$, which, in general, would cause more inhibition. Hence, more $I_{\mathrm{Na_P}}$ would be needed to compensate the increase in inhibition.

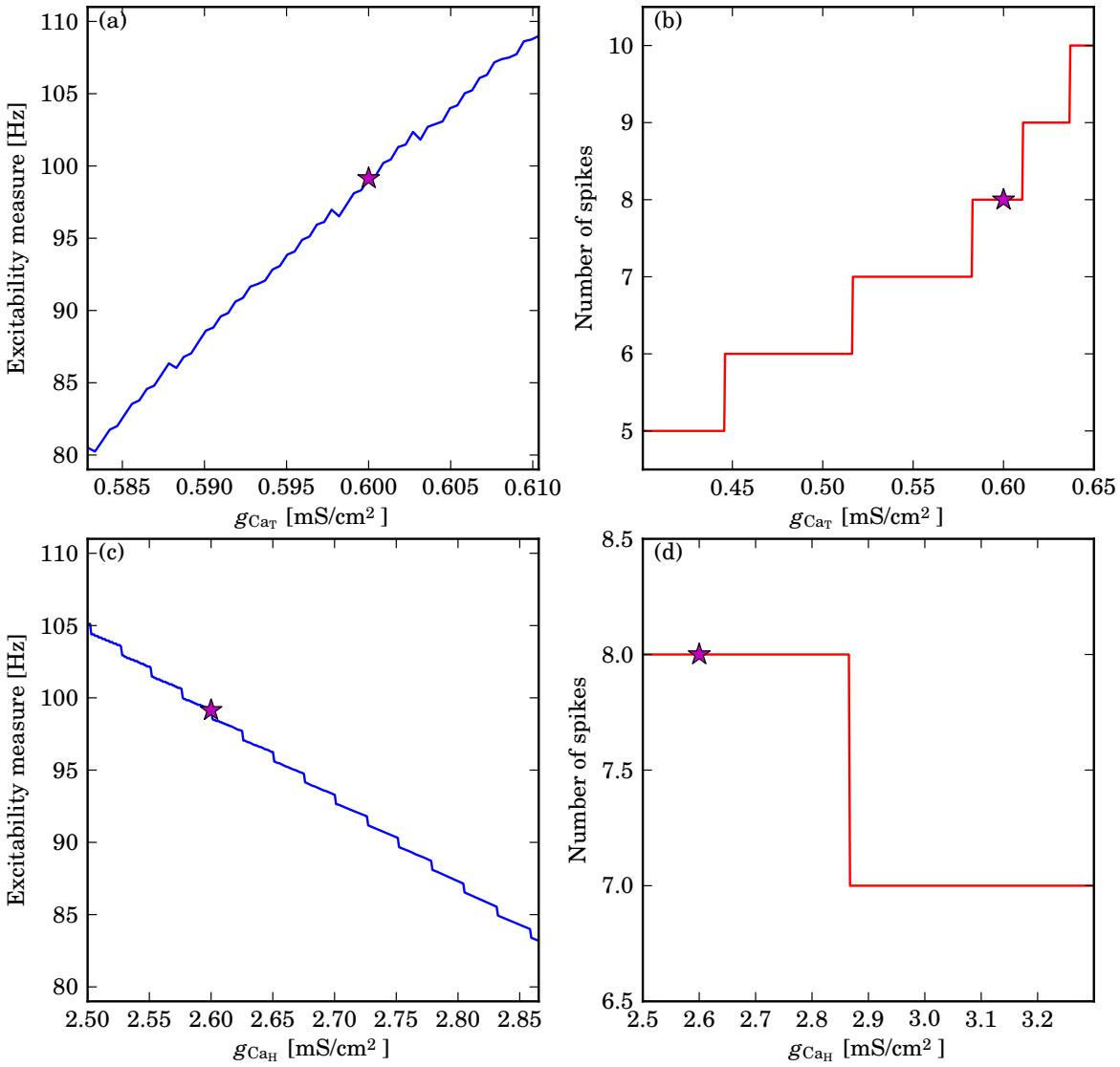

Figure 10: Parameter sensitivity analysis of the maximal conductances of the Ca^{2+}-currents; panels (a) and (c) show the excitability measure for ranges of g_{Ca_T} and g_{Ca_H}, respectively; panels (b) and (d) show the numbers of spikes in a spike train for g_{Ca_T} and g_{Ca_H}, respectively; the original values of the maximal conductances are marked by a (magenta) star.

5.3 The Ca^{2+}-channel currents

Let us now present the parameter sensitivity analysis for the inward Ca^{2+}-channel currents. The influence of the maximal conductances of these currents on the neural excitability in the model is shown in Fig. 10. The excitability measures as functions of g_{Ca_T} and of g_{Ca_H} are shown in Figs. 10(a) and (c), respectively. Figures 10(b) and (d) illustrate the changes in the numbers of spikes as the maximal conductances vary. Because of the low-voltage activation, similar to I_{Na_P}, the change of g_{Ca_T} also has a large effect on the excitability properties of the model. The excitability measure has a steep slope and reaches quite high values within a small interval of g_{Ca_T}

(Fig. 10(a)). Moreover, Fig. 10(b) illustrates that the changes in the numbers of spikes are significant for this parameter. We were able to perform the analysis only for a relatively small interval of $g_{\mathrm{Ca_T}}$; this is due to the fact that for values below $0.4\ \mathrm{mS/cm^2}$ the inhibition is too large and no action potentials are generated. On the other hand for $g_{\mathrm{Ca_T}} > 0.65\ \mathrm{mS/cm^2}$ the model exhibits bursting behaviour. Note that for the CA3 neuron model $g_{\mathrm{Ca_T}} = 0.74\ \mathrm{mS/cm^2}$, which is above the bursting boundary for the CA1 parameter set. The reason why CA3 neurons may tolerate more $I_{\mathrm{Ca_T}}$ is the higher inhibition from the outward currents. Moreover, CA3 neural responses are more excitable as far as the transient burst is concerned. These results establish the relatively high sensitivity of the model to changes in $I_{\mathrm{Ca_T}}$. Moreover, it suggests that concentrations of $\mathrm{Ca^{2+}}$ can indirectly affect the pyramidal-cell behaviour, because it can change the amount of active $I_{\mathrm{Ca_T}}$ through the Nerst potential of $\mathrm{Ca^{2+}}$. In addition, analysis of both $I_{\mathrm{Na_P}}$ and $I_{\mathrm{Ca_T}}$ shows that low-voltage activated currents, which are important elements of neural excitability, can also cause bursting of the pyramidal neuron.

The parameter sensitivity analysis of $g_{\mathrm{Ca_H}}$ produces counterintuitive results similar to those for $g_{\mathrm{Na_T}}$. Since it affects mostly the amplitudes of the action potentials, the increase of $g_{\mathrm{Ca_H}}$ results in a decrease of the excitability measure, as shown in Fig. 10(c). Note that the values of the excitability measure are not as high as for $g_{\mathrm{Ca_T}}$, which means that the frequency is less affected. This increase eventually causes a depolarised state instead of action potentials for $g_{\mathrm{Ca_H}} > 3.3$ mS/cm^2. Figure 10(d) shows that $g_{\mathrm{Ca_H}}$ has only little influence on the number of spikes.

For both CA1 and CA3 parameter sets we find equivalent effects on excitability due to changes in $g_{\mathrm{Ca_H}}$. Importantly these effects are also similar to the influence of changes in total $\mathrm{Na^+}$-current in the model. Therefore, a decrease in $g_{\mathrm{Ca_H}}$ may be the cause for hyperexcitability as well.

5.4 The $\mathrm{K^+}$-channel currents

Finally, we perform parameter sensitivity analysis of the outward currents in our model. Figure. 11 shows the influence of these maximal conductances on the behaviour of our model. Figures 11(a) and (c) depict the excitability measures as function of $g_{\mathrm{K_{DR}}}$ and $g_{\mathrm{K_M}}$, respectively. The changes in the number of spikes are show in Fig. 11(b) and (d).

Both outward currents have a significant inhibitory influence on the model excitability, as is reflected by the negative slopes of the excitability measures shown in Fig. 11(a) and (c). Note that $g_{\mathrm{K_M}}$ varies on a much smaller scale than $g_{\mathrm{K_{DR}}}$ (Fig. 11(c)). The excitability measure in Fig. 11(a) and (c) appear to have similar slopes, but small changes of $g_{\mathrm{K_M}}$ have a greater influence on the overall excitability. Evidently, small changes of $g_{\mathrm{K_M}}$ cause profound changes of both frequency and number of spikes. Moreover, the maximal values of the excitability measure are quite large compared to the previous cases, which indicates that changes of this current have a substantial effect on the spike frequency.

Figure 11(b) and (d) illustrate that both of the studied parameters have a significant impact on the number of spikes. Figure 11(d) also confirms our previous finding that a decrease of $g_{\mathrm{K_M}}$, as for the CA3 neuron model, produces a CA1-like regular spiking behaviour. Since for the CA1 parameter set the value of $g_{\mathrm{K_M}}$ is lower than for CA3, the long-lasting inhibition caused by

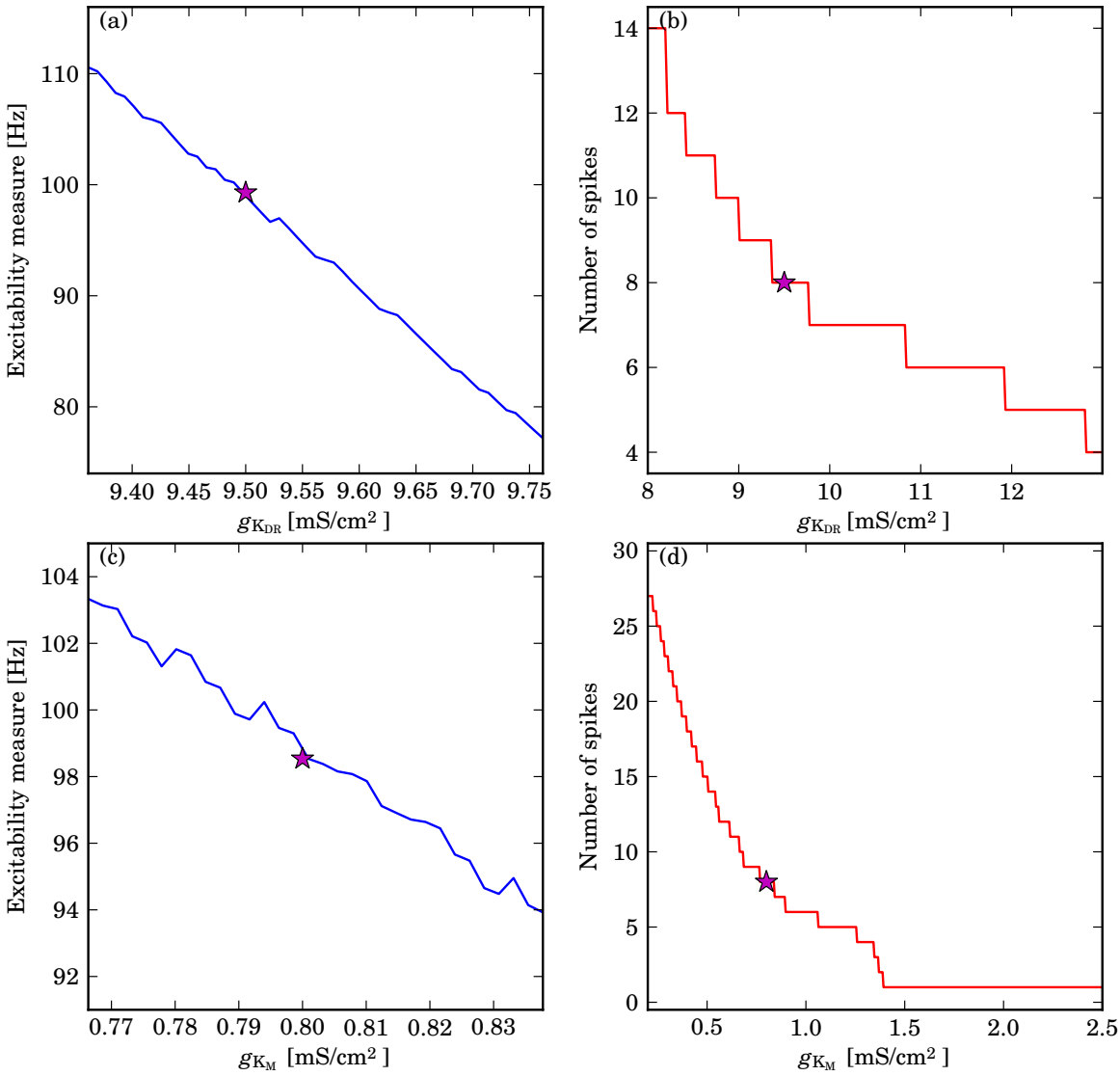

Figure 11: Parameter sensitivity analysis of the maximal conductances of the K^+-currents; panels (a) and (c) show the excitability measure for ranges of $g_{K_{DR}}$ and g_{K_M}, respectively; panels (b) and (d) show the number of spikes in a spike train for $g_{K_{DR}}$ and g_{K_M}, respectively; the original values of the maximal conductances are marked by a (magenta) star.

this current is smaller. Therefore, the amount of inward current in low-voltage region is larger, which allows the membrane potential to cross the spiking-threshold much more often. Hence, more action potentials can be generated. Moreover, because I_{K_M} is a slow current, it deactivates slowly as well. Hence, lower g_{K_M} causes less active I_{K_M} in the low-voltage region, which directly influences the inward currents.

We started the parameter sensitivity analysis from $g_{K_{DR}} = 8$ mS/cm^2, because below that value our model exhibits bursting. On the other hand, further decreases of g_{K_M} toward zero produces tonic-spiking behaviour without any bursts in the model. This could be explained by the fact that I_{K_M} is slow and has a long-lasting effect on the spiking behaviour of the model.

6 Discussion

Recent experimental studies demonstrate, that after-depolarisation is an intrinsic feature of the CA1/3 nuronal soma (Yue et al., 2005; Golomb et al., 2006; Yaari et al., 2007; Chen and Yaari, 2008; Safiulina et al., 2008; Brown and Randall, 2009). Indeed, the soma is the centre where all synaptic inputs are integrated to produce a response that could be propagated in the neural network; ADP results from this integration of the input signals. Hence, an understanding of this phenomenon is important not only from a single-cell point of view, but also from the point of view of macroscopic behaviour of neural circuits.

In this paper we presented a unified model of CA1/3 pyramidal cells that was calibrated to and validated with recent experimental data obtained at close-to-physiological temperatures. We used this model to unravel the mechanisms that govern ADP and transient bursting behaviour in these cell types. Our analysis of the model suggests a possible explanation for a number of puzzling experimental observations related to hyperexcitability in pathological conditions.

Previous theoretical studies of hippocampal pyramidal cells often used complex multi-compartmental models (Traub et al., 1991; Migliore et al., 1995; Lazarewicz et al., 2002). The first attempt of constructing a simpler pyramidal neuron model was published in (Pinsky and Rinzel, 1994), followed later by one of the most recent single-compartment models of pyramidal cell presented in (Golomb et al., 2006; Xu and Clancy, 2008). Our modelling study confirms that the responses of pyramidal neurons to short and long stimuli can be reproduced using a single-compartment model. The parameters values in our model are based on recent voltage-clamp data measured in close-to-physiological temperatures (above $30^{\circ}\mathrm{C}$). Indeed, recent studies (Liu et al., 2003; Blackmer et al., 2009; Brown and Randall, 2009) show that the time constants of the channels increase dramatically with an increase in temperature, although the parameters of (in)activation curves are similar for lower temperatures. As a result, in contrast to the previous theoretical studies of ADP (Golomb et al., 2006), our model reproduces the characteristic shape of the ADP 'hump'. Furthermore, our study shows the importance of taking into account the slow inactivations of $I_{\mathrm{Ca_H}}$ and $I_{\mathrm{K_{DR}}}$. Since $I_{\mathrm{Ca_H}}$ is a high-voltage activated current that mainly influences the amplitude of the action potential, its inactivation is responsible for the spike-amplitude modulation in the model. Interestingly, inactivation of $I_{\mathrm{K_{DR}}}$ plays a major role in the transient behaviour of the model by setting the initial value of $I_{\mathrm{K_{DR}}}$ according to the resting potential. This allows the model to reproduce the growth of the ADP as the resting potential increases. Moreover, after the resting potential exceeds -70 mV, bursts of additional spikes are fired on top of the ADP.

Our study focused on the short-term behaviour of pyramidal cell, in particular, ADP and transient bursts. Therefore, we used a minimal set of outward currents and only considered those that are important for ADP. As a consequence, our model does not reproduce the spike adaptation very well. A recent study shows that the incorporation of several additional K^{+}-currents found in pyramidal cells leeds to much better reproduction of the spike adaptation (Hemond et al., 2008). This study also suggests that slow inactivation of K^{+}-currents can reproduce the late-spiking behaviour. Hence, we expect that long-term behaviour of our model can be improved with a more versatile selection of additional slow outward currents. We showed that the slightly slower deactivation of $I_{\mathrm{Ca_T}}$ makes it a major current mediating ADP. In our model $I_{\mathrm{Na_P}}$ also plays an important role in shaping the ADP, but, due to its instantaneous gating, it is very small during

ADP. Recent studies in (Destexhe and Bal, 2009) show that $I_{\mathrm{Na_P}}$ may be a slightly slower current with an activation-time constant similar to $\tau_{m_{\mathrm{Ca_T}}}$. Such a change would slow deactivation of this current and hence increase its influence on modulation of the amplitude and duration of ADP.

We defined ADP as a local maximum of the membrane potential. We analysed this phenomenon by using the derivative dV/dt; we performed the same analysis also for the experimental measurements. This method of analysis is particularly useful in the study of onset of ADP, which corresponds to a subthreshold cubic tangency of the membrane potential to the V-nullcline. The bursting behaviour of hippocampal neurons is not only an interesting feature of the cell's physiology, it is also an essential part of the neural information processing that takes place during spatial navigation (Harvey et al., 2009). Recent experimental in-vivo studies show that bursting behaviour plays an important role in hippocampal place cells (Harvey et al., 2009). Our modelling results show that dV/dt and its nullcline play an important role in establishing of the bursting-threshold. If the difference between the inward and outward currents is sufficiently high for the membrane potential to reach -60 mV then the fast Na^+-currents are engaged and, thus, additional spikes will be generated on top of ADP.

Our sensitivity analysis of the Na^+-currents showed that a decrease of this current can result in an increase of excitability. Such increases of excitability accompanied by decreases of Na^+-currents was also observed in Alzheimer-disease animal models (our unpublished data). Moreover, recent results in (Kile et al., 2008; Misra et al., 2008) show that Na^+-currents are indeed decreased in some cases of inherited epilepsies (such as benign familial neonatal-infantile seazures, BFNIS). Hyperexcitable CA1/3 behaviour has been demonstrated (Kile et al., 2008) in an animal model of such epilepsies that is associated with sodium channel mutation (SCN2A). Interestingly, patch-clamp analysis of human tsA201 cells transfected with SCN2A mutation showed that cells expressing BFNIS mutants exhibited lower levels of sodium current (see Fig. 2A in (Misra et al., 2008)). Our sensitivity analysis suggests that high-voltage-activated Ca^{2+}-channels can cause similar hyperexcitability effects.

Acknowledgements

JN was supported by grant EP/E032249/1 from the Engineering and Physical Sciences Research Council (EPSRC), and HMO by an EPSRC Advanced Research Fellowship grant.

References

Andersen, P., Morris, R., Amaral, D., Bliss, T., O'Keefe, J., 2007. The Hippocampus Book. Oxford University Press Inc., Oxford.

Blackmer, T., Kuo, S.P., Bender, K.J., Apostolides, P.F., Trussell, L.O., 2009. Dendritic calcium channels and their activation by synaptic signals in auditory coincidence detector neurons. Journal of Neurophysiology 102, 1218–1226.

Brown, J.T., Randall, A.D., 2009. Activity-dependent depression of the spike after-depolarization generates long-lasting intrinsic plasticity in hippocampal CA3 pyramidal neurons. The Journal of Physiology 587, 1265–1281.

Chen, S., Yaari, Y., 2008. Spike Ca^{2+} influx upmodulates the spike afterdepolarization and bursting via intracellular inhibition of KV7/M channels. The Journal of Physiology 586, 1351–1363.

Destexhe, A., Bal, T., 2009. Dynamic-Clamp: From Principles to Applications. Springer, New York.

Ermentrout, B., 2002. Simulating, Analyzing, and Animating Dynamical Systems: a Guide to XPPAUT for Researchers and Students. Society for Industrial and Applied Mathematics, Philadelphia.

Golomb, D., Yue, C., Yaari, Y., 2006. Contribution of persistent Na^{+} current and M-type K^{+} current to somatic bursting in CA1 pyramidal cells: combined experimental and modeling study. Journal of Neurophysiology 96, 1912–1926.

Harvey, C.D., Collman, F., Dombeck, D.A., Tank, D.W., 2009. Intracellular dynamics of hippocampal place cells during virtual navigation. Nature 461, 941–949.

Hemond, P., Epstein, D., Boley, A., Migliore, M., Ascoli, G.A., Jaffe, D.B., 2008. Distinct classes of pyramidal cells exhibit mutually exclusive firing patterns in hippocampal area CA3b. Hippocampus 18, 411–424.

Hodgkin, A.L., Huxley, A.F., 1952. A quantitative description of membrane current and its application to conduction and excitation in nerve. The Journal of Physiology 105, 500–544.

Hunter, J., 2007. Matplotlib: a 2D graphics environment. Computing in Science & Engineering 9, 90–95.

Izhikevich, E.M., 2006. Dynamical Systems in Neuroscience: the Geometry of Excitability and Bursting. MIT Press, Cambridge, MA.

Jaffe, D.B., Ross, W.N., Lisman, J.E., Lasser-Ross, N., Miyakawa, H., Johnston, D., 1994. A model for dendritic Ca^{2+} accumulation in hippocampal pyramidal neurons based on fluorescence imaging measurements. Journal of Neurophysiology 71, 1065–1077.

Kile, K.B., Tian, N., Durand, D.M., 2008. Scn2a sodium channel mutation results in hyperexcitability in the hippocampus in vitro. Epilepsia 49, 488–499.

Lazarewicz, M.T., Migliore, M., Ascoli, G.A., 2002. A new bursting model of CA3 pyramidal cell physiology suggests multiple locations for spike initiation. BioSystems 67, 129–137.

Liu, Z., Ren, J., Murphy, T.H., 2003. Decoding of synaptic voltage waveforms by specific classes of recombinant high-threshold Ca^{2+} channels. The Journal of Physiology 553, 473–488.

Migliore, M., Cook, E., Jaffe, D., Turner, D., Johnston, D., 1995. Computer simulations of morphologically reconstructed CA3 hippocampal neurons. Journal of Neurophysiology 73, 1157–1168.

Misra, S.N., Kahlig, K.M., Jr, A.L.G., 2008. Impaired NaV1.2 function and reduced cell surface expression in benign familial neonatal-infantile seizures. Epilepsia 49, 1535–1545.

Naundorf, B., Wolf, F., Volgushev, M., 2006. Unique features of action potential initiation in cortical neurons. Nature 440, 1060–1063.

Nowacki, J., 2010. XPPy, A Python package for simulations in XPPAUT (Ermentrout, 2002). available via http://seis.bris.ac.uk/˜enxjn/xppy.

Oldfield, S., Hancock, J., Mason, A., Hobson, S.A., Wynick, D., Kelly, E., Randall, A.D., Marrion, N.V., 2009. Receptor-mediated suppression of potassium currents requires colocalization within lipid rafts. Molecular Pharmacology 76, 1279–1289.

Oliphant, T., 2007. Python for scientific computing. Computing in Science & Engineering 9, 10–20.

Pinsky, P.F., Rinzel, J., 1994. Intrinsic and network rhythmogenesis in a reduced Traub model for CA3 neurons. Journal of Computational Neuroscience 1, 39–60.

Safiulina, V.F., Zacchi, P., Taglialatela, M., Yaari, Y., Cherubini, E., 2008. Low expression of Kv7/M channels facilitates intrinsic and network bursting in the developing rat hippocampus. The Journal of Physiology 586, 5437–5453.

Scharfman, H.E., 1993. Spiny neurons of area CA3c in rat hippocampal slices have similar electrophysiological characteristics and synaptic responses despite morphological variation. Hippocampus 3, 9–28.

Traub, R., Wong, R., Miles, R., Michelson, H., 1991. A model of a CA3 hippocampal pyramidal neuron incorporating voltage-clamp data on intrinsic conductances. Journal of Neurophysiology 66, 635–650.

Wong, R.K., Prince, D.A., 1981. Afterpotential generation in hippocampal pyramidal cells. Journal of Neurophysiology 45, 86–97.

Xu, J., Clancy, C., 2008. Ionic mechanisms of endogenous bursting in CA3 hippocampal pyramidal neurons: A model study. PLoS ONE 3(4), e2056. doi:10.1371/journal.pone.0002056.

Yaari, Y., Yue, C., Su, H., 2007. Recruitment of apical dendritic T-type Ca^{2+} channels by back-propagating spikes underlies de novo intrinsic bursting in hippocampal epileptogenesis. The Journal of Physiology 580, 435–450.

Yue, C., Remy, S., Su, H., Beck, H., Yaari, Y., 2005. Proximal persistent Na^{+} channels drive spike afterdepolarizations and associated bursting in adult CA1 pyramidal cells. Journal of Neuroscience 25, 9704–9720.

Yue, C., Yaari, Y., 2004. KCNQ/M channels control spike afterdepolarization and burst generation in hippocampal neurons. Journal of Neuroscience 24, 4614–4624.

Yue, C., Yaari, Y., 2006. Axo-somatic and apical dendritic Kv7/M channels differentially regulate the intrinsic excitability of adult rat CA1 pyramidal cells. Journal of Neurophysiology 95, 3480–3495.